GDAŃSK UNIVERSITY OF TECHNOLOGY
FACULTY OF ELECTRICAL AND CONTROL ENGINEERING
DEPARTMENT OF ELECTRIC DRIVES AND ENERGY CONVERSION

Sensorless Five-Phase Induction Motor Drive with Inverter Output Filter and Fault Detection Possibility

Patryk D. Strankowski

Supervisor:
Assoc. Prof. Jarosław Guziński, D.Sc.

Auxiliary Supervisor:
Marek Adamowicz, Ph.D.

Gdańsk, 2019

Table of contents

1 Introduction

Adjustable speed AC motor drives have attracted increasing attention in recent decades as the preferred choice of electric energy conversion for industrial and transport applications. Significant advances in the power electronics field allowed the implementation of sophisticated control methods for electrical drives. The application of voltage source inverters in conjunction with various control concepts, e.g. field oriented control (FOC) [1], [2], direct toque control (DTC) [3], multiscalar control [4] provides a great energy saving potential, increases the maximum motor efficiency usage, as well as improves the drive system durability.

Nevertheless, the reliability and efficiency of a drive system depend not only on the control structure and inverter technology, but also on the condition of the machine and the mechanical system. For this reason, the industry is interested in long-lasting and fault tolerant drive systems, especially those with high responsibility, and in single-unit production drives for special applications.

Multiphase machines are gaining an increasing popularity due to their advantages over three-phase machines, e.g. reduced per phase power rating, improved reliability, and increased degrees of freedom [5]–[7]. Compared with three-phase AC drives, variable speed multiphase drives provide a higher power range by utilizing low-power switching devices, due to the higher number of inverter phase legs and higher torque density. These properties are in particular important for applications in which power supply voltage is limited, torque oscillation amplitude decrease is necessary, and/or greater fault-tolerant ability is required. The fault-tolerance capability is one of the most attractive properties of multiphase machines for industrial applications [6]. This especially includes drive systems with high reliability in non-stop operation conditions that are known for high economical and safety repercussions caused by fault occurrence, e.g. in electrical vehicles [7], traction [8], ship propulsion [9], offshore wind farms, and other safety-critical applications such as electrical helicopters [7].

1.1 Five-Phase Induction Motors

The first publication about a five-phase drive concept was in 1969 by Ward and Härer [10]. Nevertheless, the interest in multiphase drives (with a phase number higher than three) was limited, for the reason that three-phase machines were dominant and extensively popular in the industry, and the costs of a multiphase system were not standing in relation with their advantages. However, the progress of power electronics and microprocessors, with simultaneous decrease of their prices, raised the interest in multiphase drives in the beginning of the 1980s.

Among others, the advantages provided by five-phase induction motors compared to their three-phase counterparts include [11], [12]:

- higher reliability due to the higher phase number,
- smaller electromagnetic torque pulsations and lower noise level,
- better stator material use through the utilisation of the 3rd current harmonic,
- smaller rated transistor current in the voltage source inverter due to the division of the current into more phases.

The most important advantage is the higher reliability that ensures an uncritical operation, and even possible start-up, of the induction motor with one or two nonadjacent opened phases. The only drawback here is that the torque which provides a possibility for operation with open phases is paid with current increase in the remaining phases. However, this current increase is significantly lower than in three-phase induction motors.

The beforementioned improvement in the stator material use is possible through the addition of an extra current harmonic, namely the 3rd harmonic injection [11]. The idea behind it is to obtain a quasi-rectangular rotor flux distribution, as presented in Fig. 1.1.

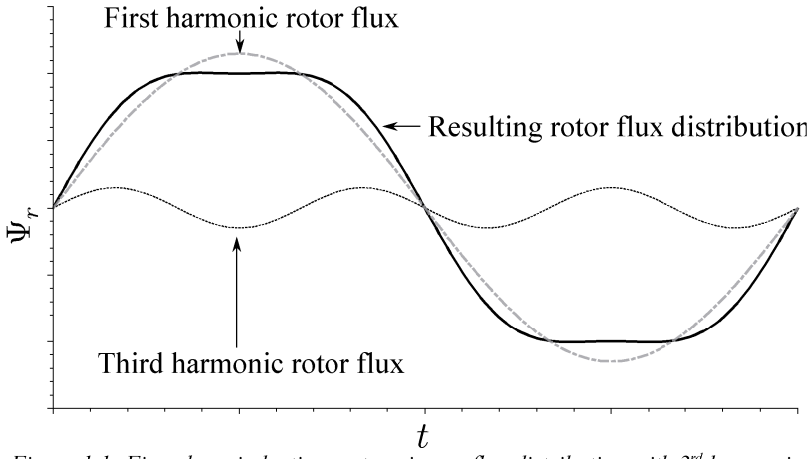

Figure 1.1: Five phase induction motor air gap flux distribution with 3rd harmonic injection

The addition of the 3rd harmonic to the fundamental harmonic leads to a resulting rotor flux distribution with lower peak value compared to the sinusoidal flux distribution (Fig. 1.1).

However, during the same period, the peak value of the quasi-rectangular distribution is longer in the pre-saturation range than that of the sinusoidal distribution, which tends towards better overall usage of the magnetic circuit. The principle of constructive harmonic injection can be applied to all multiphase drives, with the restriction that all harmonic numbers above the machine phase number generate losses and some torque pulsations [11].

For a five-phase machine, the 3rd harmonic utilization is possible through the Clarke transformation from five phases into two orthogonal subsystems, as denoted in Eq. (1.1).

$$\begin{bmatrix} i_{\alpha 1} \\ i_{\beta 1} \\ i_{\alpha 3} \\ i_{\beta 3} \\ i_o \end{bmatrix} = \sqrt{\frac{2}{5}} \begin{bmatrix} 1 & \cos\left(\frac{2\pi}{5}\right) & \cos\left(\frac{4\pi}{5}\right) & \cos\left(\frac{4\pi}{5}\right) & \cos\left(\frac{2\pi}{5}\right) \\ 0 & \sin\left(\frac{2\pi}{5}\right) & \sin\left(\frac{4\pi}{5}\right) & -\sin\left(\frac{4\pi}{5}\right) & -\sin\left(\frac{2\pi}{5}\right) \\ 1 & \cos\left(\frac{4\pi}{5}\right) & \cos\left(\frac{8\pi}{5}\right) & \cos\left(\frac{8\pi}{5}\right) & \cos\left(\frac{4\pi}{5}\right) \\ 0 & \sin\left(\frac{4\pi}{5}\right) & \sin\left(\frac{8\pi}{5}\right) & -\sin\left(\frac{8\pi}{5}\right) & -\sin\left(\frac{4\pi}{5}\right) \\ \frac{1}{\sqrt{2}} & \frac{1}{\sqrt{2}} & \frac{1}{\sqrt{2}} & \frac{1}{\sqrt{2}} & \frac{1}{\sqrt{2}} \end{bmatrix} \cdot \begin{bmatrix} i_a \\ i_b \\ i_c \\ i_d \\ i_e \end{bmatrix} \tag{1.1}$$

As Eq. (1.1) indicates, the five-phase currents can be transformed into two orthogonal subsystems and a zero component, which allows independent consideration of both systems with respect to the harmonics. **For this reason, the system analysed in the thesis is named the 1st and 3rd harmonics system, or the 1st and 2nd orthogonal plane system.**

The transformation matrix allows to use the 2nd plane to control a second in series-connected induction, instead of one single machine with concentrated windings. The schematic representation from the view of the inverter is demonstrated in Fig. 1.2 [23], [24].

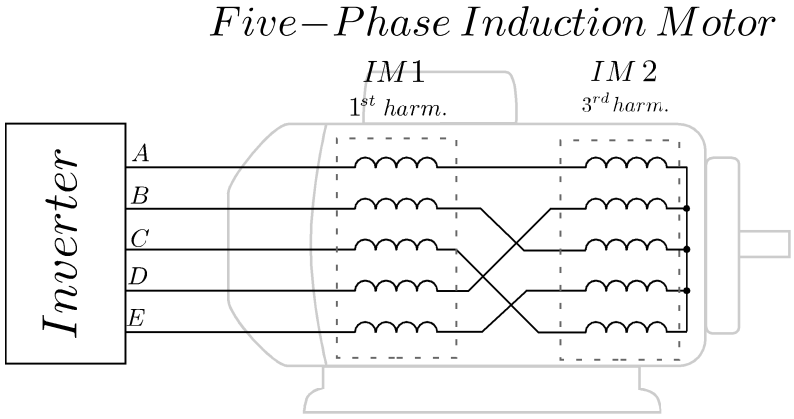

Figure 1.2: Schematic representation of the concept of five-phase induction motor control with 3rd harmonic injection

The physical five-phase induction motor is divided into two independent virtual machines (Fig. 1.2). These machines are physically connected to one drive shaft. However, as might be expected, in order to beneficially introduce the torque enhancement of the 2nd plane machine, both rotor flux components have to be synchronised together. All further necessary relations and procedures required for the implementation of a single five-phase induction motor drive with 3rd harmonic injection are presented in further sections.

1.2 Inverter Output Filters

The invention of the voltage source inverter enables, in conjunction with vector modulation techniques, a wide versatility of voltage generation and control possibilities. Nevertheless, the high voltage raise dV/dt of the modulated voltage introduces the problem of meaningful parasitic current flow, among others, through the bearings and stator winding insulations of the induction motor. This issue is especially important in drive systems with long supply cables, such as elevator systems, cranes, and ventilation systems, as well as in drive systems in explosion-proof areas. A longer cable provides higher cable inductance and cable capacitance, which in effect generate voltage interferences that increase the stresses in the motor stator insulation. Further issues related to the high voltage raise include increased electromagnetic disturbances that can influence the operation of other devices.

The structure of the LC filter for a five-phase induction motor is presented in Fig. 1.3.

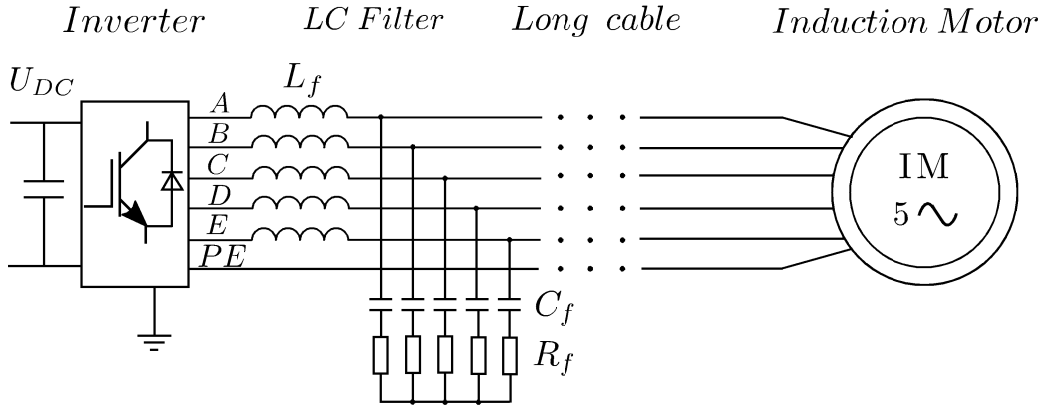

Figure 1.3: Structure of LC filter with damping resistance in the five-phase drive system

The LC filter (Fig. 1.3) is in principle a low-pass filter in each phase that consists of filter inductance L_f and filter capacitance C_f. The resistances R_f in the capacitor path play the role of dumping resistances which protect the system against resonances.

Hence, the application of the LC filter consists in filtering the inverter output voltage, which as a result changes the shape from rectangular to sinusoidal. This way, a voltage raise limitation is gained, with simultaneous reduction of the current flow through the parasitic capacitances.

The dV/dt limitation and the resultant reduction of the parasitic current flow are beneficial for the stator insulation and motor bearings, as well as for the EMI disturbance behaviour in the drive system.

Nevertheless, the additional components generate a voltage phase shift, as well as a voltage drop over the filter inductance. For this reason, a more complex control system is required, compared to a filter-less drive system, due to the filter model considered in the calculations.

1.3 Concept of Sensorless Control

For a drive system in closed-loop operation, the information of all controlled variables is mandatory. The induction motor variables which are used for precise control include rotor speed, rotor flux, stator current, stator voltage, electromotive force, and torque. In most cases, the measurement of some of these variables is uneconomic and difficult to realise.

At the same time, their calculation based on mathematical models is imaginable, but every practical mathematical model is based on simplifications that will introduce errors in computations. For this reason, observers are used for variables that are difficult to obtain, while the mathematical model is used in conjunction with the feedback of the measured variable to reduce the error between the model and reality to a lowest possible level.

A very popular control structure configuration is based on the measurements of the stator currents, and the DC-link voltage for the stator voltage information, and the rotor speed which is used as the reference signal and provides direct feedback about the drive conditions. When removing the rotor speed sensor, the drive is called speed sensorless or sensorless.

The speed observers in sensorless drives estimate the rotor speed based on the available sensors installed by default in commercially available voltage source inverters that measure the inverter output current and the DC-link voltage.

Hence, the challenge here is selecting an observer with stable properties that will estimate the desired variables in a wide operating range of rotor speed and load torque changes. Moreover, a sensorless control drawback has to be overcome that refers to the response of the estimation procedure to parameter changes caused by high temperature, transitions through zero frequency at speed reverse, and especially very low speed of operation that causes estimation problems due to low phase current values recorded in the measurement.

For the purpose of an overview of the sensorless configuration with LC filter, Fig. 1.4 illustrates a schematic representation of the drive system based on this configuration.

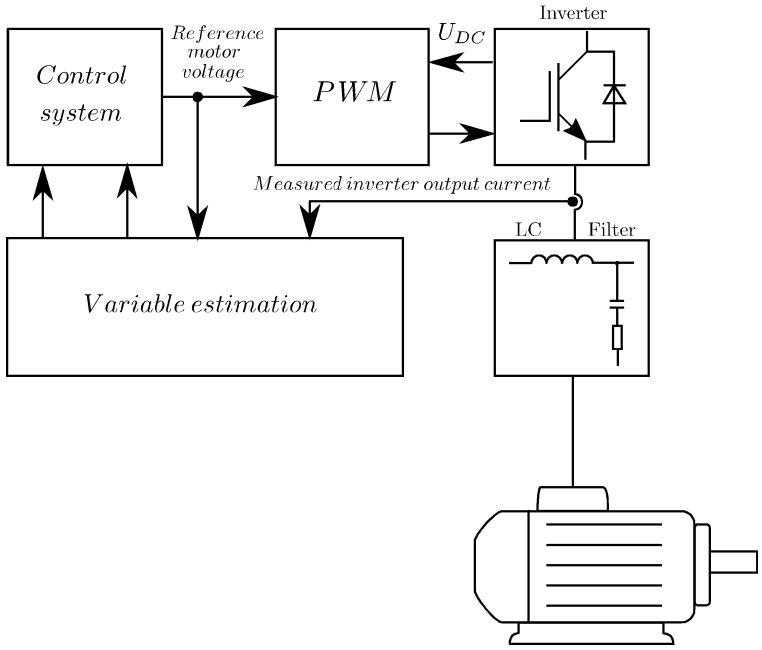

Figure 1.4: Schematic signal representation of the sensorless drive system with induction motor and inverter output filter

1.4 Thesis and Objectives

The main objective of the present work is to gain new knowledge on the development of the sensorless five-phase induction motor drive with inverter output filter, and in the field of fault detection methods. The developed drive system is assumed to be based on the five-phase topology with voltage source inverter, LC filter, and induction motor. The control makes use of multiscalar variables in sensorless configuration, which means that all necessary control signals are estimated based on the indications of the stator current sensors and DC-link voltage sensors installed in the five-phase voltage source inverter. Fault detection is performed based on the estimated variables through the speed or load torque observer procedure, with no additional sensors.

In order to reach the above formulated objectives, the following research tasks have to be executed:

- Developing a mathematical model of the five-phase induction motor drive with 3rd harmonic injection and inverter output filter.
- Implementing a simulation model of the five-phase induction motor with 3rd harmonic injection and inverter output filter.
- Experimental implementation and verification of space vector modulation with independent voltage control for the 1st and 2nd plane control systems.
- Developing a control system structure for the five-phase induction motor drive with inverter output filter that is able to handle the 2nd plane control system with rotor flux synchronisation.
- Selecting suitable observers for sensorless control of the five-phase system with inverter output filter, which will include the stability analysis for a single operation point and the assessment of variable estimation errors.
- Experimental implementation of the complete sensorless drive with inverter output filter.
- Theoretical examination of the selected observers with regard to fault detection possibilities, including frequency responses of the observers.
- Experimental verification of fault detection possibilities with the use of the implemented observers.

Based on the beforementioned objectives, the thesis is formulated as follows:

"The application of sensorless multiscalar control in the five-phase induction motor drive system with inverter output filter guarantees utilisation of the 3rd harmonic injection through rotor flux synchronisation of the 1st and 3rd harmonics, and provides reuse of the estimated state variables for potential fault detection purposes."

2 Control of Five-Phase Induction Motor

2.1 Sensorless Multiscalar Control with Third Harmonic Injection

The multiscalar model for the five-phase squirrel cage induction motor is in principle equal to the three-phase induction motor approach, but implemented for two independent multiscalar subsystems.

In order to obtain the quasi-trapezoidal rotor flux distribution described in Sec. 1.1, the 3rd harmonic has to be injected. That means that in order to obtain full independent control of the 1st and 3rd harmonics, the control system has to be divided into two parts, separately for each plane, i.e. the 1st and 2nd orthogonal plane. This also indicates that the multiscalar control has to be implemented twice, which means that the state variable estimation has to be prepared for different machine parameters in each plane. Moreover, an indepentent voltage generation for both control planes has to be implemented to allow a truly indepentent control of both machines. As mentioned before in Sec. 1.1, the transformation given by Eq (1.1) allows such separation.

As the state variable estimation of both machines is ensured, the two rotor fluxes estimated in the 1st and 2nd plane have to be synchronised together to obtain the desired resultant quasi-trapezoidal rotor flux distribution. This requires the implementation of an additional synchronisation subsystem to handle the rotor flux angle synchronisation at two different speeds.

The first implementation of the multiscalar variable based sensorless control was presented in [13]. Further versions, prepared with author's contribution, were described in [14], [15] (without LC filter) and in [16], [17] (with inverter output filter).

A schematic representation of the control structure is shown in Fig. 2.1.

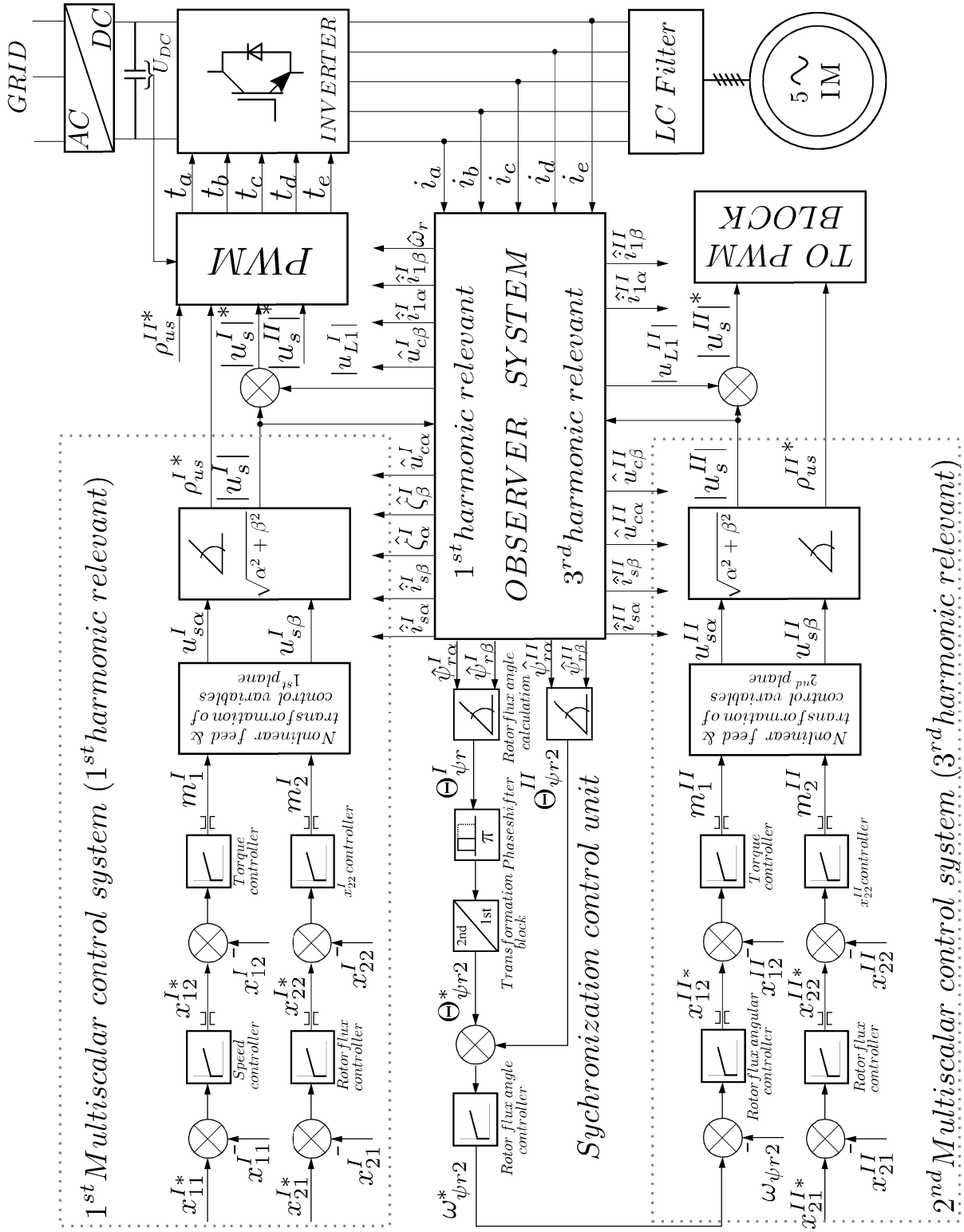

Figure 2.1: Control structure of multiscalar control of the five-phase machine with LC filter and 3rd harmonic injection

Fig. 2.1 illustrates the implemented multiscalar control structure for each subsystem, in the 1st and 2nd plane. The 1st machine control plane, i.e. the fundamental harmonic (superscript I) utilises the reference of the main rotor speed x_{11}^{*I} and the x_{21}^{*I} value, which is analogous to the rotor flux. The related PI controller outputs deliver the desired values x_{12}^{*I} (motor torque) and x_{22}^{*I} (scalar product of stator current and rotor flux vector components).

The nonlinear transformations of the control variables m_1^I and m_2^I deliver the desired voltage vectors for the PWM, which are then transformed into vector magnitude and angle. Since an LC filter is installed, the estimated inductance voltage drop is added to the desired voltage vector magnitude to compensate the voltage drop on the filter inductance.

The operation of the synchronisation unit involves calculating the rotor flux angles for both control planes. Since the 3rd harmonic is operating at the three times higher frequency than the 1st harmonic, the rotor flux angle is adapted to that with an (optional) phase shift and transformation in order to align the 1st and 3rd harmonic flux angles.

In this approach, the two rotor flux angles are synchronised through a PI controller which delivers the desired rotor flux angle speed $\omega_{\psi r2}^*$ to the input of the x_{12}^{II} controller in the 2nd plane. This structure replaces the speed controller in the 2nd control structure, because the rotor flux angle speed controller serves the same purpose as the rotor speed controller for maintenance of synchronisation. This way, independent control of both rotor flux components is possible in order to synchronise them together and to obtain the resultant quasi-trapezoidal rotor flux distribution.

Moving further through the structure, the desired square of the rotor flux value x_{21}^{*II}, the scalar product of the current and rotor flux vectors x_{22}^{*II}, the nonlinear transformation, and the consideration of the filter inductance voltage drop consideration, remain identical as in the 1st plane structure.

2.2 LC Filter Consideration in the Control System

The inverter output filter has to be considered not only in the observer, but also in the control system to ensure reliable drive operation. However, the solution to overcome this problem which is proposed in [18], [19] requires an additional subordinate control system, with coordinate transformation and further four PI controllers for the three-phase induction motor. That means that the application of that solution in two control planes, which is the case of the five-phase induction motor drive, will require consideration of eight additional PI controllers (sum for both, the 1st and 2nd control system).

The concept presented in [16], [17] is based on multiscalar variables and simplifies the calculation effort to four PI controllers. Although the above solution offers good control properties, it requires more PI controller tuning. This increases the level of complexity and involves much more computing time, which is very limited in the microprocessor. To be able to accomplish the main tasks of the thesis, the author had found a compromise solution which reduced the computational effort of the LC filter control.

That is why a solution was proposed to reduce the calculation capacities required for the 1st and 2nd plane estimations, based on filter inductance voltage drop calculations, as denoted in Eq. (2.1).

$$\hat{u}_{1\alpha}^{(i)} = L_f \frac{d\hat{i}_{1\alpha}^{(i)}}{d\tau} \quad , \quad \hat{u}_{1\beta}^{(i)} = L_f \frac{d\hat{i}_{1\beta}^{(i)}}{d\tau} \tag{2.1}$$

The filter current differentials of $i_{1\alpha}$ and $i_{1\beta}$, calculated each time in the observer and passed to the Runge-Kutta integration routine, are used to calculate the magnitude of the resulting voltage drop on the filter inductance. This approach makes it possible to calculate the magnitude of the filter inductance voltage drop.

However, it is known that the differentials are sensitive to fast changes which are likely to occur in several drive conditions, e.g. at speed and load torque changes. To limit these unwanted effects, the filtration was used as denoted in Eq. (2.2):

$$|U_{1F}|^{(i)} = \left(L_f \cdot \sqrt{\frac{\hat{di_{1\alpha}}}{dt}^{(i)2} + \frac{\hat{di_{1\beta}}}{dt}^{(i)2}} - |U_{1F}|^{(i)} \right) \cdot k_f \tag{2.2}$$

where $|U_1|^{(i)}$ is the inductance voltage drop in the inverter output filter, $U_{1F}^{(i)}$ is a temporary variable for filtering the differentials and considered in the SVM, L_f is the filter inductance, and k_f is the filter coefficient.

The additional filtration allows to calculate the magnitude of the voltage drop on the filter inductance, which then can be added to the desired voltage of the control system before the execution of the PWM routine. This voltage drop compensation serves as support of the control system in both planes. For a better understanding, the overall structure of the control system support is shown in Fig. 2.2

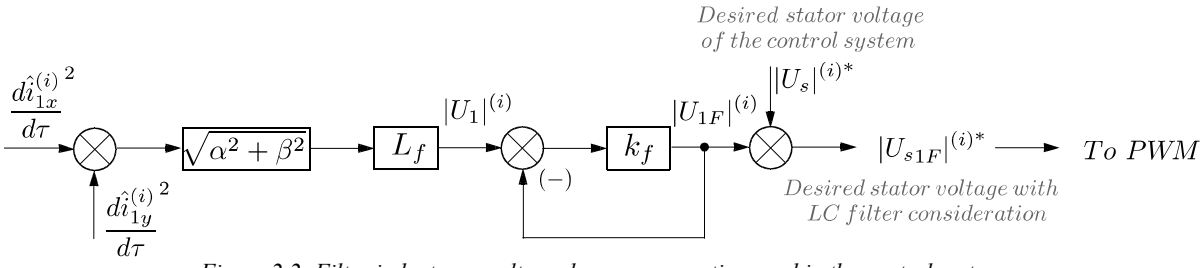

Figure 2.2: Filter inductance voltage drop compensation used in the control system

Summarising this procedure, it should be mentioned that this voltage drop consideration is not the most optimal solution, compared to the solutions with the utilisation of PI controllers, mainly due to the fact that the concern of the phase shift between inverter output and motor input is not addressed.

However, the experimental results have shown that in this particular case the voltage drop consideration helped the drive system to overcome the main difficulty related to the presence of the filter with very low computational effort, which was the compromise that had to be made in the experiment, and was an essential prerequisite for putting the drive into operation.

3 Speed and Rotor Flux Observers for Sensorless Control of Five-Phase Induction Motor with LC Filter

3.1 Speed Observer for First Plane System

In order to obtain the control solely based on the measured phase currents and DC-link voltage, all variables required for the control have to be estimated, including the rotor flux, rotor speed, and electromotive force. The accuracy of estimation through state observers determines the quality and possibilities of control without additional speed sensors.

Each control plane requires special focus, i.e. a speed observer is required for the 1st plane, while a rotor flux observer is sufficient for the 2nd plane.

A speed observer that has proved to provide an accurate rotor speed estimation is the speed observer with disturbance model developed by Krzemiński, where the EMF serves as an auxiliary variable and is treated as a disturbance.

The successfully implemented speed observer in [20] was initially used for drive systems without inverter output filter. However, an additional filter element which causes voltage drop on filter inductance has to be considered in sensorless control. A speed observer with inverter output filter model was described in [18], [21], where the capacitor voltage drop was calculated as denoted in Eq. (3.1):

$$u_c = \int \frac{i_1 - i_s}{C_f} d\tau \tag{3.1}$$

The application of Eq. (3.1) to the speed observer structure is conceivable. However, a real test setup is a source of uncertainties, e.g. noise, and/or limited calculation precision, that have to be considered and handled. Successful experimental implementation of Eq. (3.1) was presented in [18], but the success in this case depends, in general, on the applied speed observer structure, drive system, and current filtration during the experiment.

To minimise the unwanted effects during the capacitor voltage calculation, a feedback loop was added to the structure, as presented in Fig. 3.1.

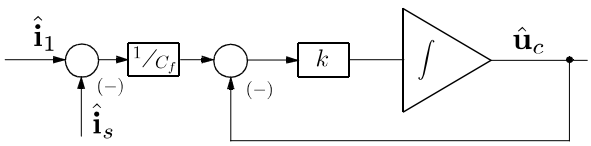

Figure 3.1: Structure of the capacitor voltage drop calculation with integrator output feedback

The introduction of this feedback and the notation as differential equation lead to Eq. (3.2), which is used to calculate the capacitor voltage drop.

$$\frac{du_c}{d\tau} = \left(\frac{i_1 - i_s}{C_f} - u_c \right) \cdot k \tag{3.2}$$

Here, k is the gain that determines the influence of filtering.

This obtained structure is according to the structure of the 1st order lag element (PT1) [22] and introduces lag in the calculations. Moreover, the structure introduces a filtering effect, which is desired to limit the negative integrator influences.

An analogous approach was applied by the authors in [23]–[25] to a rotor flux estimator, and was referred to as 1st order lag circuit. This method improved the estimation for sensorless controlled drives, especially in low frequency ranges. In [26], [27] the authors presents further corresponding solutions to estimate the flux components, to mention only a few.

However, the feedback enhancement also introduces a filtering effect, which depends on the frequency and generates an additional observer estimation error, especially in the higher frequency range. The above approach introduced by the author is an indispensable compromise to provide reliable estimation calculations which, at the same time, should be fast enough under experimental conditions to handle the control procedures.

The presented speed observer is based on the speed observer structure with complete model of disturbances, which was presented by Krzemiński in [28] for three-phase drives without inverter output filter, and modified by Guziński in [18], [21] with consideration of the inverter output filter. The author's contribution includes the modification of the capacitor voltage calculation with feedback, embedding the stator voltage calculation into the stator current estimation (this calculation was performed in separate steps in [29]), and the introduction of the modified observer into the five-phase drive system. The speed observer estimates the stator current, rotor flux, EMF, capacitor voltage, filter inductor current, and rotor speed, and is given by Eqs. (3.3) – (3.13):

$$\frac{d\hat{i}_{s\alpha}}{d\tau}^{(I)} = a_1^{(I)} \cdot \hat{i}_{s\alpha}^{(I)} + a_2^{(I)} \cdot \hat{\psi}_{r\alpha}^{(I)} + a_3 \cdot \hat{\zeta}_{\beta}^{(I)} + a_4^{(I)} \cdot (\hat{u}_{c\alpha}^{(I)} + (\hat{i}_{1\alpha}^{(I)} - \hat{i}_{s\alpha}^{(I)}) \cdot R_f) + k_1^{(I)} \cdot (\hat{i}_{1\alpha}^{(I)} - i_{1\alpha}^{(I)}) \tag{3.3}$$

$$\frac{d\hat{i}_{s\beta}}{d\tau}^{(I)} = a_1^{(I)} \cdot \hat{i}_{s\beta}^{(I)} + a_2^{(I)} \cdot \hat{\psi}_{r\beta}^{(I)} - a_3^{(I)} \cdot \hat{\zeta}_{\alpha}^{(I)} + a_4^{(I)} \cdot (\hat{u}_{c\beta}^{(I)} + (\hat{i}_{1\beta}^{(I)} - \hat{i}_{s\beta}^{(I)}) \cdot R_f) + k_1^{(I)} \cdot (\hat{i}_{1\beta}^{(I)} - i_{1\beta}^{(I)}) \tag{3.4}$$

$$\frac{d\hat{\psi}_{r\alpha}}{d\tau}^{(I)} = a_5^{(I)} \cdot \hat{\psi}_{r\alpha}^{(I)} + a_6^{(I)} \cdot \hat{i}_{s\alpha}^{(I)} - \hat{\zeta}_{\beta}^{(I)} + k_2^{(I)} \cdot (\hat{\zeta}_{\beta}^{(I)} - \hat{\omega}_r \cdot \hat{\psi}_{r\beta}^{(I)}) \tag{3.5}$$

$$\frac{d\hat{\psi}_{r\beta}}{d\tau}^{(I)} = a_5^{(I)} \cdot \hat{\psi}_{r\beta}^{(I)} + a_6^{(I)} \cdot \hat{i}_{s\beta}^{(I)} + \hat{\zeta}_{\alpha}^{(I)} - k_2^{(I)} \cdot (\hat{\zeta}_{\alpha}^{(I)} - \hat{\omega}_r \cdot \hat{\psi}_{r\alpha}^{(I)}) \tag{3.6}$$

$$\frac{d\hat{\zeta}_{\alpha}}{d\tau}^{(I)} = a_5^{(I)} \cdot \hat{\zeta}_{\alpha}^{(I)} - \hat{\omega}_r \cdot \hat{\zeta}_{\beta}^{(I)} - a_6^{(I)} \cdot \hat{i}_{s\alpha}^{(I)} \cdot \hat{\omega}_r + k_3^{(I)} \cdot (\hat{i}_{1\alpha}^{(I)} - i_{1\alpha}^{(I)}) \tag{3.7}$$

$$\frac{d\hat{\zeta}_{\beta}}{d\tau}^{(I)} = a_5^{(I)} \cdot \hat{\zeta}_{\beta}^{(I)} + \hat{\omega}_r \cdot \hat{\zeta}_{\alpha}^{(I)} - a_6^{(I)} \cdot \hat{i}_{s\beta}^{(I)} \cdot \hat{\omega}_r + k_3^{(I)} \cdot (\hat{i}_{1\beta}^{(I)} - i_{1\beta}^{(I)}) \tag{3.8}$$

$$\frac{d\hat{u}_{c\alpha}}{d\tau}^{(I)} = \left(\frac{(\hat{i}_{1\alpha}^{(I)} - \hat{i}_{s\alpha}^{(I)})}{C_f} - \hat{u}_{c\alpha}^{(I)} \right) \cdot k_4^{(I)} \tag{3.9}$$

$$\frac{d\hat{u}_{c\beta}}{d\tau}^{(I)} = \left(\frac{(\hat{i}_{1\beta}^{(I)} - \hat{i}_{s\beta}^{(I)})}{C_f} - \hat{u}_{c\beta}^{(I)} \right) \cdot k_4^{(I)} \tag{3.10}$$

$$\frac{d\hat{i}_{1\alpha}}{d\tau}^{(I)} = \frac{u_{s\alpha}^{*(I)} - R_{ind} \cdot \hat{i}_{1\alpha}^{(I)} - R_f \cdot (\hat{i}_{1\alpha}^{(I)} - \hat{i}_{s\alpha}^{(I)}) - \hat{u}_{c\alpha}^{(I)}}{L_f} + k_5^{(I)} \cdot (\hat{i}_{1\alpha}^{(I)} - i_{1\alpha}^{(I)}) + k_6^{(I)} \cdot (\hat{i}_{1\beta}^{(I)} - i_{1\beta}^{(I)}) \tag{3.11}$$

$$\frac{d\hat{i}_{1\beta}}{d\tau}^{(I)} = \frac{u_{s\beta}^{*(I)} - R_{ind} \cdot \hat{i}_{1\beta}^{(I)} - R_f \cdot (\hat{i}_{1\beta}^{(I)} - \hat{i}_{s\beta}^{(I)}) - \hat{u}_{c\beta}^{(I)}}{L_f} + k_5^{(I)} \cdot (\hat{i}_{1\beta}^{(I)} - i_{1\beta}^{(I)}) - k_6^{(I)} \cdot (\hat{i}_{1\beta}^{(I)} - i_{1\beta}^{(I)}) \tag{3.12}$$

$$\hat{\omega}_r = \frac{\hat{\zeta}_\alpha^{(I)} \hat{\psi}_{r\alpha}^{(I)} + \hat{\zeta}_\beta^{(I)} \hat{\psi}_{r\beta}^{(I)}}{\hat{\psi}_{r\alpha}^{2(I)} + \hat{\psi}_{r\beta}^{2(I)}} \tag{3.13}$$

where $\hat{i_s}$ is the estimated stator current, $\hat{\psi}_r$ is the estimated rotor flux, $\hat{\zeta}$ is the estimated EMF , $\hat{u_c}$ is the estimated voltage drop on the filter capacitance, $\hat{i_1}$ is the estimated filter inductance current, $\hat{\omega_r}$ is the estimated rotor speed, R_{ind} and R_f are the inductance and filter resistances, respectively, $k_1 ... k_6$ are observer gains, and $a_1 ... a_6$ are variables obtained from the induction motor model.

The observer gains were initially selected based on empirical approach during the simulation process, and then fine-tuned during the experiment.

3.2 Rotor Flux Observer for Second Plane System

To take advantage of the 3rd harmonic injection, the sensorless control of the 2nd machine requires an additional observer, which has to be adapted to the needs of the 2nd plane.

In order to address this concern, a complete speed observer, which was mandatory for the 1st plane, is not required in the case of the 2nd plane. The most important state variable in the 2nd plane is the rotor flux, the role of which is to guarantee the synchronisation with the 1st plane control system, and to enable the generation of the desired quasi-trapezoidal rotor flux distribution. Hence, the speed estimation of the 2nd plane machine can be omitted, what is beneficial in terms of computation time limitation.

However, the implementation of the 2nd plane observer provides a challenge, since the 2nd plane machine operates with a nominal frequency of 150 Hz, i.e. three times as high as that of the 1st plane observer.

Analogously to the 1st plane speed observer, the 2nd plane rotor flux observer also requires consideration of the LC filter.

As might be expected, the 1st plane speed observer, the space vector modulation, and the control system occupied most of the available calculation time in the microprocessor during the experiment. Thus, the 2nd plane rotor flux observer had to be implemented in as minimalistic form as possible, but

simultaneously had to be able to deliver sufficiently accurate and stable properties to guarantee faultless synchronisation with the 1st plane. The right selection of this observer was mandatory to accomplish the tasks formulated in the thesis.

In order to address this concern, the author selected a Luenberger rotor flux observer, which was presented by Krzemiński [30] without LC filter consideration. A modified version of this observer with respect to the inverter output filter is presented in [18]. The author extended the observer structure with the presented capacitor voltage calculation, embedded the stator voltage calculation into the stator current equation, and modified it by using one observer gain coefficient in the inductance current estimation to reduce the effort of coefficient selection.

All this being denoted by Eqs. (3.14) – (3.22).

$$\frac{d\hat{i}_{s\alpha}}{d\tau}^{(II)} = a_1^{(II)} \cdot \hat{i}_{s\alpha}^{(II)} + a_2^{(II)} \cdot \hat{\psi}_{r\alpha}^{(II)} + a_3^{(II)} \cdot \hat{\psi}_{r\beta}^{(II)} \cdot \hat{\omega}_r^{II} + a_4^{(II)} \cdot (\hat{u}_{c\alpha}^{(II)} + (\hat{i}_{1\alpha}^{(II)} - \hat{i}_{s\alpha}^{(II)}) \cdot R_f) + k_1^{(II)} \cdot (\hat{i}_{1\alpha}^{(II)} - i_{1\alpha}^{(II)}) \quad (3.14)$$

$$\frac{d\hat{i}_{s\beta}}{d\tau}^{(II)} = a_1^{(II)} \cdot \hat{i}_{s\beta}^{(II)} + a_2^{(II)} \cdot \hat{\psi}_{r\beta}^{(II)} - a_3^{(II)} \cdot \hat{\psi}_{r\alpha}^{(II)} \cdot \hat{\omega}_r^{II} + a_4^{(II)} \cdot (\hat{u}_{c\beta}^{(II)} + (\hat{i}_{1\beta}^{(II)} - \hat{i}_{s\beta}^{(II)}) \cdot R_f) + k_1^{(II)} \cdot (\hat{i}_{1\beta}^{(II)} - i_{1\beta}^{(II)}) \quad (3.15)$$

$$\frac{d\hat{\psi}_{r\alpha}}{d\tau}^{(II)} = a_5^{(II)} \cdot \hat{\psi}_{r\alpha}^{(II)} + a_6^{(II)} \cdot \hat{i}_{s\alpha}^{(II)} - \hat{\omega}_r^{II} \cdot \hat{\psi}_{r\beta}^{(II)} + k_2^{(II)} \cdot (\hat{i}_{1\alpha}^{(II)} - i_{1\alpha}^{(II)}) - k_3^{(II)} \cdot \hat{\omega}_r^{II} \cdot (\hat{i}_{1\alpha}^{(II)} - i_{1\alpha}^{(II)}) \quad (3.16)$$

$$\frac{d\hat{\psi}_{r\beta}}{d\tau}^{(II)} = a_5^{(II)} \cdot \hat{\psi}_{r\beta}^{(II)} + a_6^{(II)} \cdot \hat{i}_{s\beta}^{(II)} + \hat{\omega}_r^{II} \cdot \hat{\psi}_{r\alpha}^{(II)} + k_2^{(II)} \cdot (\hat{i}_{1\beta}^{(II)} - i_{1\beta}^{(II)}) - k_3^{(II)} \cdot \hat{\omega}_r^{II} \cdot (\hat{i}_{1\beta}^{(II)} - i_{1\beta}^{(II)}) \quad (3.17)$$

$$\frac{d\hat{u}_{c\alpha}}{d\tau}^{(II)} = \left(\frac{(\hat{i}_{1\alpha}^{(II)} - \hat{i}_{s\alpha}^{(II)})}{C_f} - \hat{u}_{c\alpha}^{(II)} \right) \cdot k_4^{(II)} \quad (3.18)$$

$$\frac{d\hat{u}_{c\beta}}{d\tau}^{(II)} = \left(\frac{(\hat{i}_{1\beta}^{(II)} - \hat{i}_{s\beta}^{(II)})}{C_f} - \hat{u}_{c\beta}^{(II)} \right) \cdot k_4^{(II)} \quad (3.19)$$

$$\frac{d\hat{i}_{1\alpha}}{d\tau}^{(II)} = \frac{u_{s\alpha}^{*(II)} - R_{ind} \cdot \hat{i}_{1\alpha}^{(II)} - R_f \cdot (\hat{i}_{1\alpha}^{(II)} - \hat{i}_{s\alpha}^{(II)}) - \hat{u}_{c\alpha}^{(II)}}{L_f} + k_5^{(II)} \cdot (\hat{i}_{1\alpha}^{(II)} - i_{1\alpha}^{(II)}) \quad (3.20)$$

$$\frac{d\hat{i}_{1\beta}}{d\tau}^{(II)} = \frac{u_{s\beta}^{*(II)} - R_{ind} \cdot \hat{i}_{1\beta}^{(II)} - R_f \cdot (\hat{i}_{1\beta}^{(II)} - \hat{i}_{s\beta}^{(II)}) - \hat{u}_{c\beta}^{(II)}}{L_f} + k_5^{(II)} \cdot (\hat{i}_{1\beta}^{(II)} - i_{1\beta}^{(II)}) \quad (3.21)$$

$$\hat{\omega}_r^{II} = -3\hat{\omega}_r^{I} \quad (3.22)$$

where $\hat{i_s}$ is the estimated stator current, $\hat{\psi}_r$ is the estimated rotor flux, $\hat{\zeta}$ is the estimated EMF, $\hat{u_c}$ is the estimated voltage drop on the filter capacitance, $\hat{i_1}$ is the estimated filter inductance current, R_{ind} and R_f are the inductance and filter resistances, respectively, $k_1 ... k_5$ are observer gains, and $a_1 ... a_6$ are variables obtained from the induction motor model.

Here, the observer's coefficients were also selected based on empirical approach during the simulation, and then fine-tuned during the drive launch.

3.3 Load Torque Observer

To address the concern of a fault detection possibility, without using additional sensors beyond the sensors that are installed by default in comercial voltage source inverters, the author introduced a further load torque observer as source of additional information about the drive condition and abnormality detection. For this a reduced-order load torque observer was implemented that is based on Gopinath's approach. The utilisation of this concept reduces beneficially the computational effort, compared to a full state observer.

The complete load torque observer with estimated rotor speed takes the form of Eqs. (3.23) and (3.24):

$$\frac{d\mathbf{z}}{dt} = \begin{bmatrix} 0 & -k_{1L} \\ 1 & -k_{2L} \end{bmatrix} \mathbf{z} + \begin{bmatrix} k_{1L}k_{2L}J_M \\ \left(k_{2L}^2 - k_{1L}\right) J_M \end{bmatrix} \hat{\omega}_r + \begin{bmatrix} k_{1L} \\ k_{2L} \end{bmatrix} \hat{T}_e \tag{3.23}$$

$$\hat{T}_L = z_2 - k_{2L}J_M\hat{\omega}_r \tag{3.24}$$

where $\hat{T}_L$ is the estimated motor load torque, $\mathbf{z} = \begin{bmatrix} z_1 & z_2 \end{bmatrix}^T$ is the load torque observer internal state vector, $\hat{T}_e$ is the calculated motor electromagnetic torque, k_{1L}, k_{2L} are the observer coefficients, J_M is the inertia, and $\hat{\omega}_r$ is the estimated angular rotor speed. The gains k_{1L} and k_{2L} were chosen based on empirical approach, in which the estimated load torque had to be as close as possible to the load torque applied in the simulation.

4 Experimental Investigations of the Drive System

4.1 Evaluation of Experimental Results

This section presents experimental running capabilities of the drive in several drive conditions. Most drive system relevant variables are presented, including the multiscalar variables of the 1st and 2nd control planes, the rotor flux vector components, the resulting rotor flux distribution, and synchronisation related variables. Importance is attached to rotor flux synchronisation and to the speed estimation error during several drive operations

Each motor start-up from zero is performed with V/f control, in order to ensure the stabilisation of the estimated state variables. After the stabilisation sequence, the control system is automatically switched to sensorless control. All PI controller parameters have been fine-tuned for different drive situations, in order to present the best operation conditions of the drive.

The section concludes with the summary of the outcome gained from the experiments.

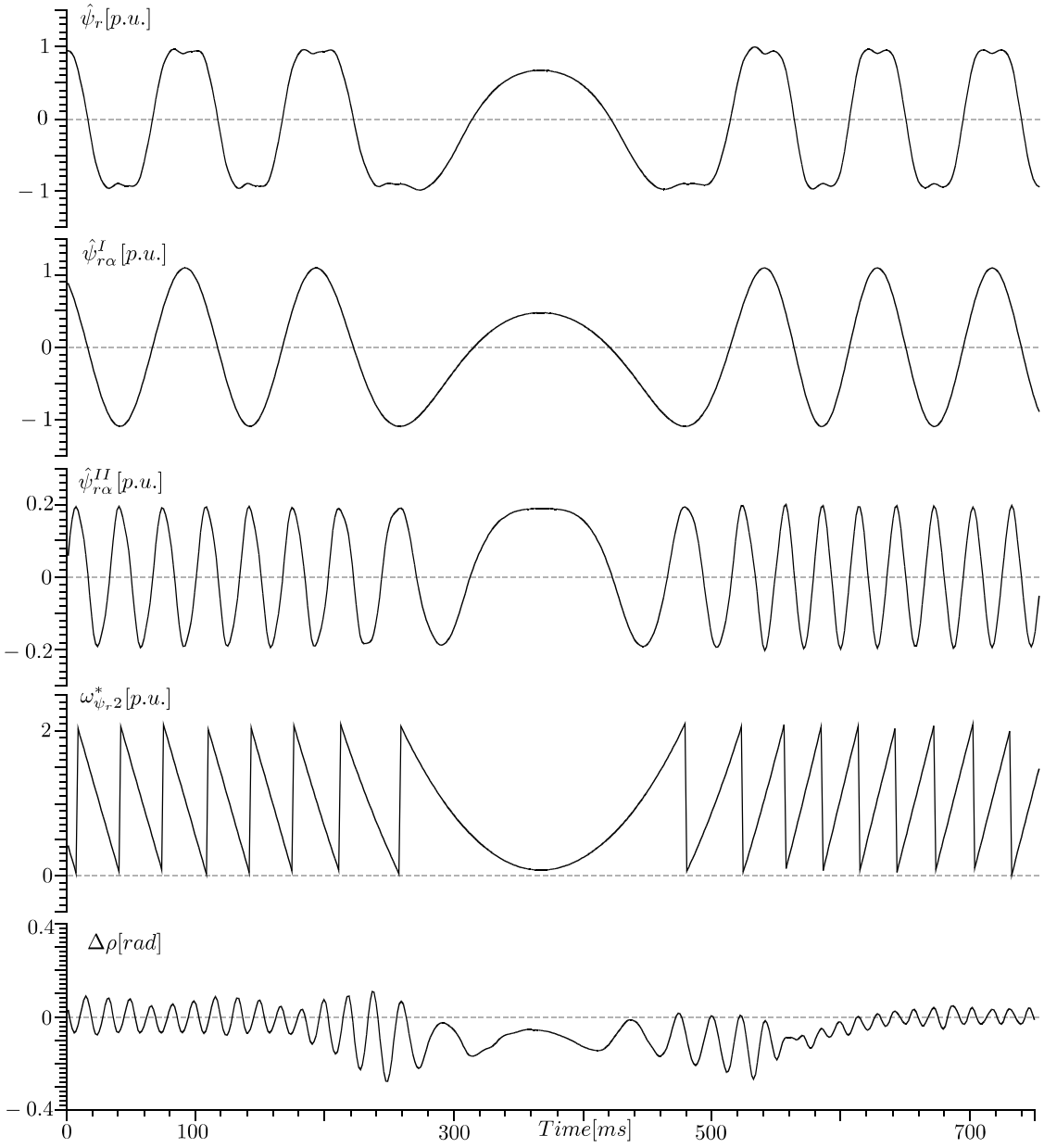

Figure 4.1: Estimated resulting rotor flux, rotor flux vector components for the 1st and 2nd plane, rotor flux angle, and synchronisation error – speed reverse.

Fig. 4.1 illustrates the estimated resulting rotor flux distribution $\hat{\psi}_r$, the rotor flux component for the 1st and 2nd plane $\hat{\psi}^I_{r\alpha}$ $\hat{\psi}^{II}_{r\alpha}$, the output value of the rotor flux angle speed controller $\omega^*_{\psi r2}$, and the synchronisation error $\Delta\rho$, which were recorded during motor direction reverse from ω_r = 0.2 p.u. to – 0.2 p.u.

Noticeable here is the maintenance of the quasi-trapezoidal flux distribution during the complete sequence. The zero transition causes no negative effects, the rotor flux vector components in the 1st and 2nd planes are interacting smoothly, even in the lower speed range, and the synchronisation error oscillations do not exceed a peak value of 0.3 rad.

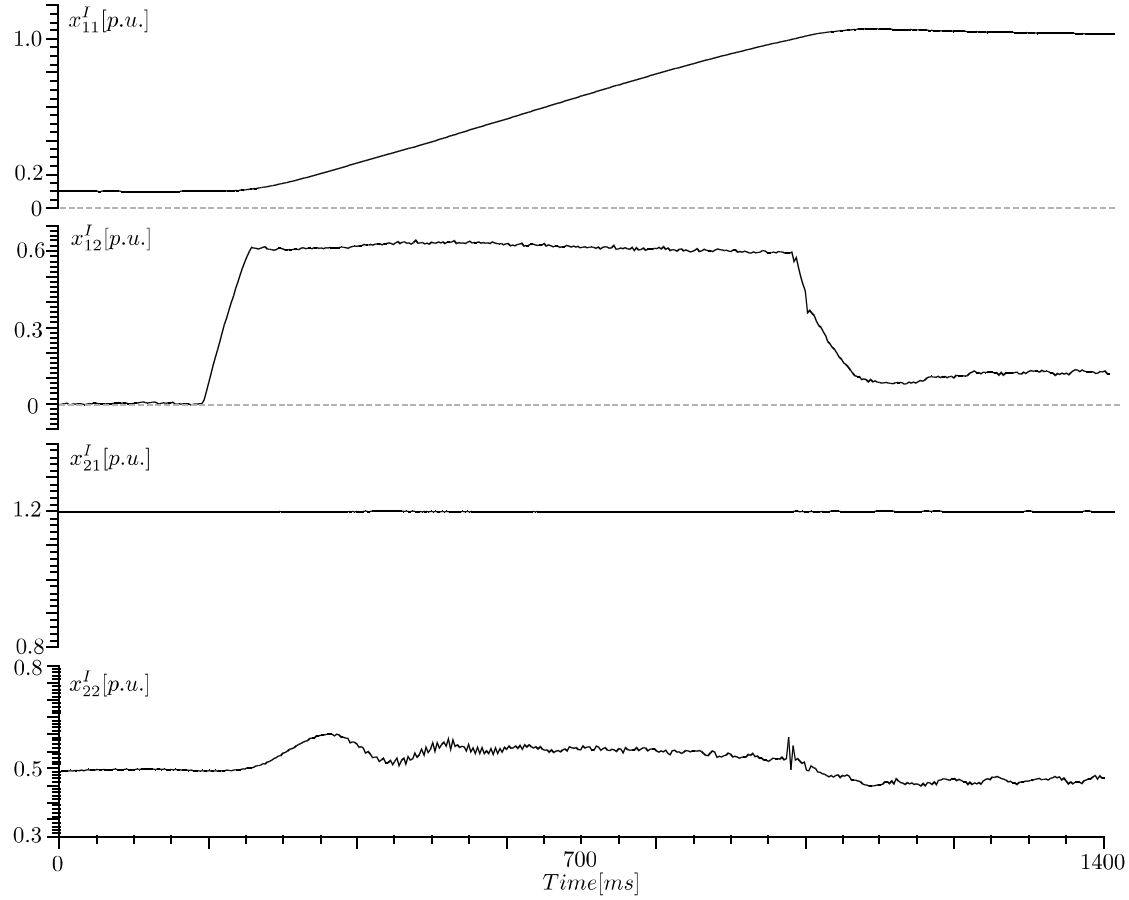

Figure 4.2: Multiscalar variables in the 1st control plane – speed change

Fig. 4.2 demonstrates changes of the multiscalar variables in the 1st plane during speed change from ω_r = 0.1 p.u. to 1.0 p.u. As can be seen, the speed change causes a step change of the x_{12}^I value, which is analogous to the torque, and maintains its steady value of about 0.62 p.u. This value is the determined load torque limitation for this sequence, which was assumed to reduce the acceleration during the speed change. This was especially important for ensuring good synchronisation of the 2nd plane rotor flux. An abrupt speed change may cause loss of synchronisation.

The variable x_{21}^I maintains the determined desired value of about 1.2 p.u. in all presented drive conditions. The variable x_{22}^I maintains the mean value of about 0.5 p.u, but reveals some oscillations with maximum peak values of 0.1 p.u. and 0.05 p.u., but with no negative effects.

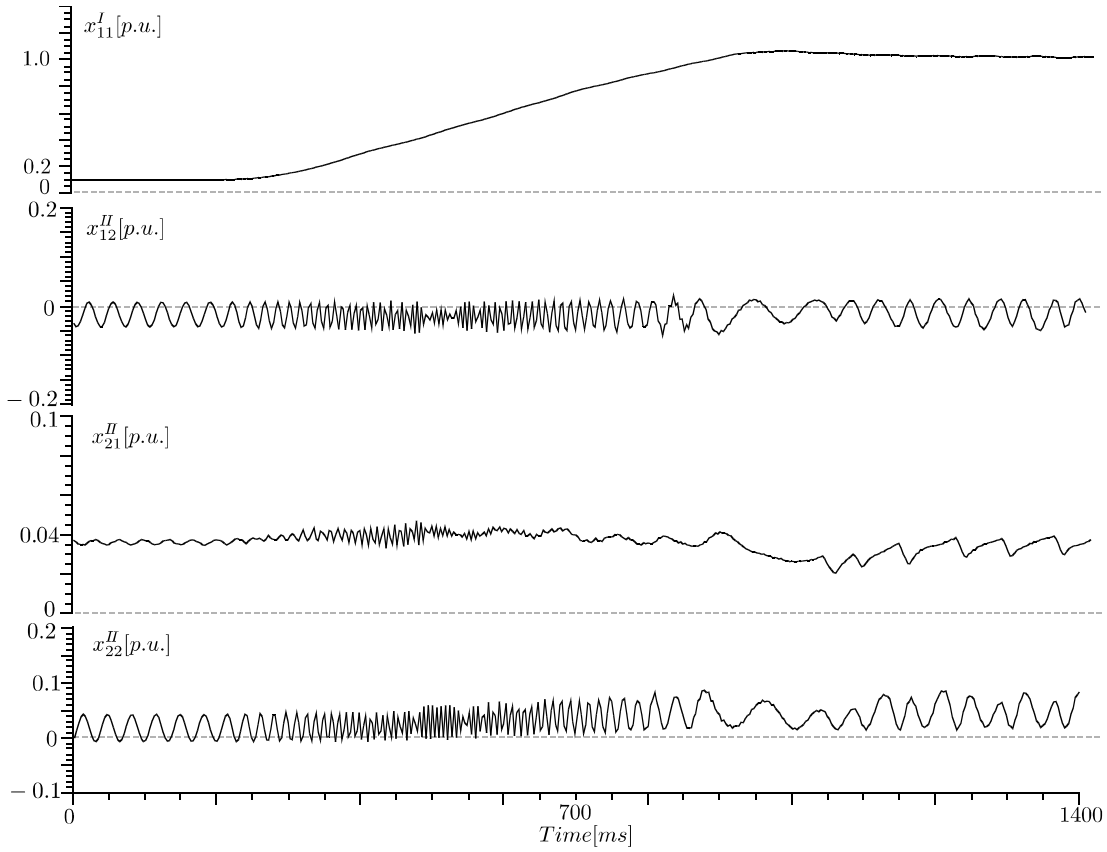

Figure 4.3: Multiscalar variables in the 2nd control plane – speed change

Fig. 4.3 demonstrates changes of the 2nd plane multiscalar variables during speed change from ω_r = 0.1 p.u. to 1.0 p.u., in identical conditions as in the experiment presented in Fig. 4.2.

The variable x_{12}^{II} reveals some oscillations. However, they are limited to the negative range of up to – 0.05 p.u., which is necessary to obtain a positive torque on the drive shaft.

The variable x_{21}^{II} also oscillates, but maintains the average value of 0.035 p.u., as determined in the control. The variable x_{22}^{II} behaves like the other variables and has a similar waveform as x_{12}^{II}.

The observed oscillations are probably caused by calculation inaccuracies of the control when estimating the observer variables. It has to be mentioned here that it was a great challenge to handle the small value range of the estimated variables at the three times higher frequency of the control system than the nominal rotor frequency, i.e. 150 Hz against 50 Hz.

Apart from visible oscillations of the multiscalar variables, the quasi-trapezoidal rotor flux distribution has been maintained in the complete drive operation range, which was the goal of introducing the 2nd control system.

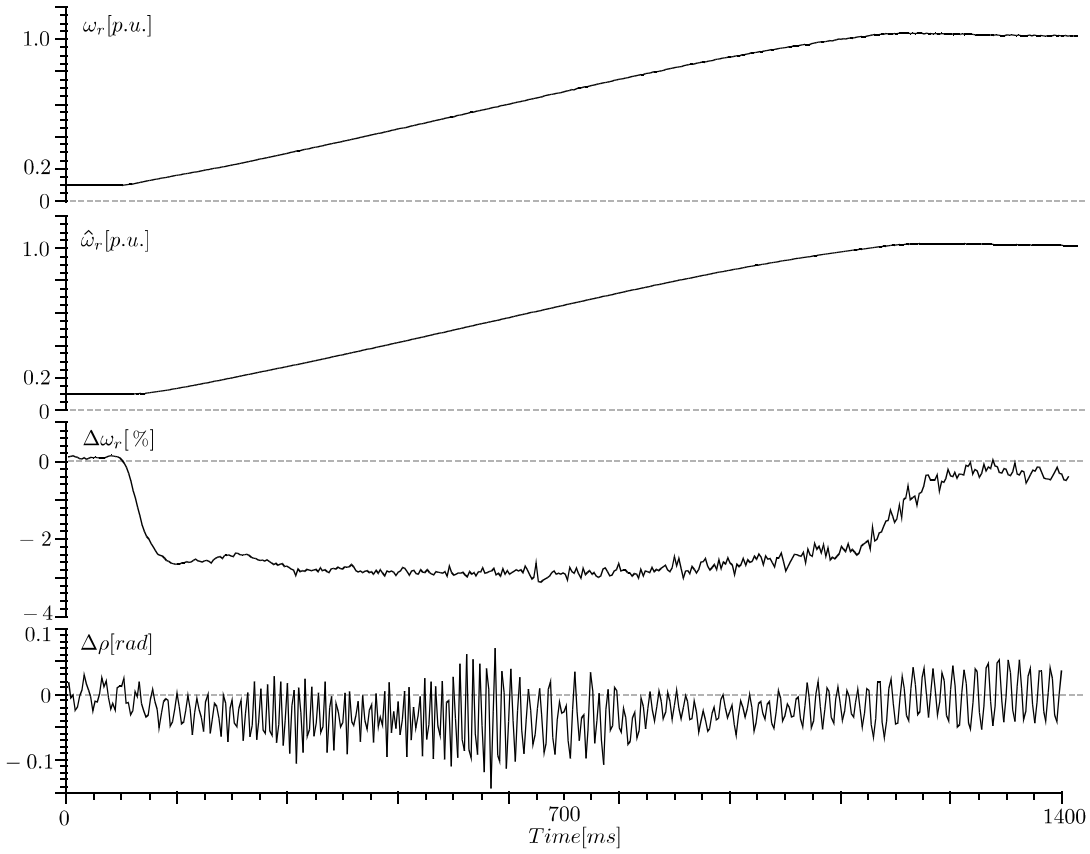

Figure 4.4: Measured rotor speed, estimated rotor speed, speed estimation error, and synchronization error – speed change

Fig. 4.4 shows the measured speed ω_r, the estimated speed $\hat{\omega}_r$, the estimation error $\Delta\omega_r$, and the synchronisation error $\Delta\rho$ during motor speed change from ω_r = 0.1 p.u. to 1.0 p.u., after synchronisation.

As can be seen, the speed estimation error $\Delta\omega_r$ reaches the maximum of about 2.5% at the beginning of speed change, and decreases steadily to less than 1%.

The synchronisation error is also at a low level, of approx. 0.07 rad, and generates no negative effects to the synchronisation.

The vulnerable point of each sensorless drive is low speed operation at low frequency. Low voltages and frequencies close to zero are the source of problems for the estimation procedure, which may result in unstable operation of the entire control system.

Fig. 4.5 presents the effects of speed reverse from ω_r = 0.02 p.u. to –0.02 p.u., including the estimated rotor flux distribution $\hat{\psi}_r$, the estimated rotor speed $\hat{\omega}_r$, and the synchronisation error $\Delta\rho$.

As can be seen, the synchronisation is preserved, and the quasi-trapezoidal flux distribution $\hat{\psi}_r$ is maintained even at this speed range, which is remarkable when considering the low voltage, of about 0.006 p.u., in the 2nd plane. The synchronisation error oscillates in the range of 0.2 p.u., and has no negative effects on the drive operation.

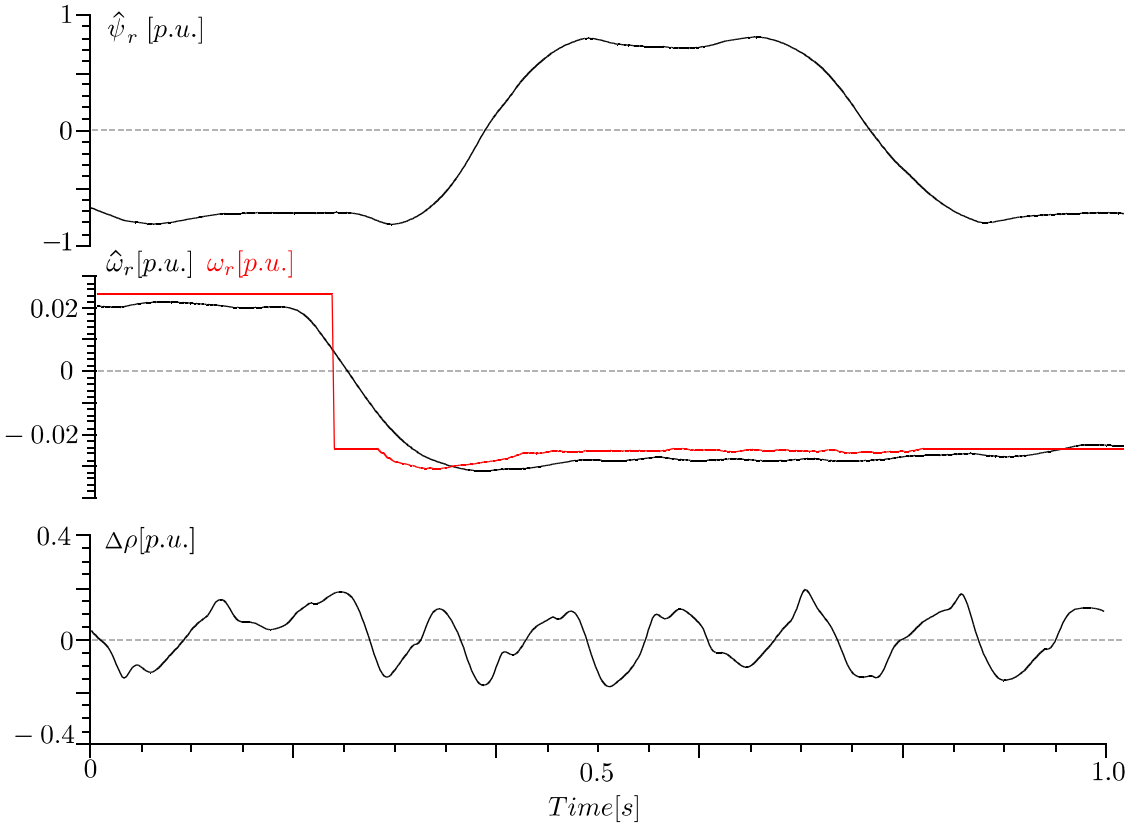

Figure 4.5: Total rotor flux, measured rotor speed, estimated rotor speed, and synchronisation error – speed reverse from ω_r = 0.02 p.u. to – 0.02 p.u.

Both the control system, and the speed estimation remain stable, even at zero transition when the maximal speed estimation error is about 19%. However, it recovers, as can be seen in the last sequence of the illustration. It has to be mentioned here that due to hardware limitation, the speed measurement ω_r can be considered incorrect, especially in the zero speed/frequency transition zone, as can be concluded from the step change at the approx. 250 ms.

The final experiment addresses the torque improvement gained through the 3rd harmonic injection to the control system with the presented configuration.

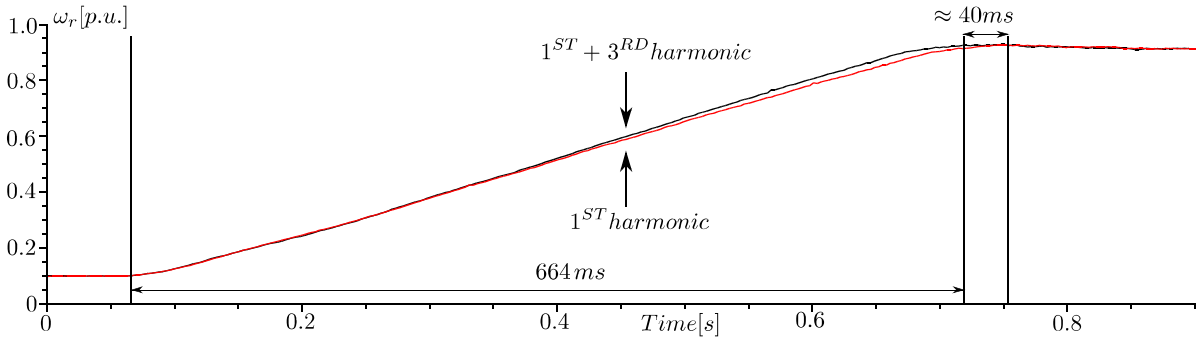

Figure 4.6: Comparing rotor speeds for the 1st harmonic only (red) and 1st + 3rd harmonic injection (black) – motor speed change

Fig. 4.6 presents the rotor speed measured during speed change from ω_r = 0.1 p.u. to 0.9 p.u., without (red) and with 3rd harmonic injection (black).

As the comparison shows, the desired speed is reached about 40ms faster with the 3rd harmonic injection, which means the 6% improvement in this particular case. This improvement can be seen analogous to the torque enhancement gained through the 3rd harmonic injection.

It is worth mentioning here that other related works without LC filter also recorded an improvement when applying multiscalar control [15] (ca. 10% torque increase), sensorless FOC control, with author's contribution [31] (ca. 10% torque improvement), and DTC [32] (ca. 10% increase).

In conclusion, the drive system worked well in sensorless operation. The transition through zero frequency did not cause any negative effects. The estimation error of the rotor speed was at a very low level in steady-state conditions, which is remarkable when considering that the calculations were based only on the measurement of the inverter output phase currents and the DC-link voltage.

The multiscalar control and the flux estimation and synchronisation of both rotor flux components worked stably.

Nevertheless, the running of the complete drive structure was only possible with complex PI controllers tuning in both planes. Handling of the variable estimation and control in the 2nd plane has proved to be a challenging task, due to the relatively high frequency that can cause problems, and the relatively small values of the variables.

However, the main objective, which was running the drive system in sensorless operation with five-phase induction motor with LC filter and 3rd harmonic injection, has been successfully archived.

5 Drive Capabilities Under Fault Conditions

5.1 Observer Investigations with Major Drive Disturbances

This section presents the observer investigation of simulated drive disturbances of major significance, which means that these disturbances can affect globally the operation of the drive. The idea behind the disturbance simulation allows generating disturbances of different nature, which can represent virtual faults in the mechanical system without the need to introduce real mechanical faults to the drive. These faults can be related to unbalances and misalignment of the drive shaft, and faults in the transmission system.

Fig. 5.1 presents the test setup for the disturbance generation. For this, two induction machines were used, each with nominal power of 5.5 kW. The load machine serves as the disturbance generator and is equipped with the rotor speed measurement system. The other machine is the tested five-phase machine, controlled in sensorless configuration.

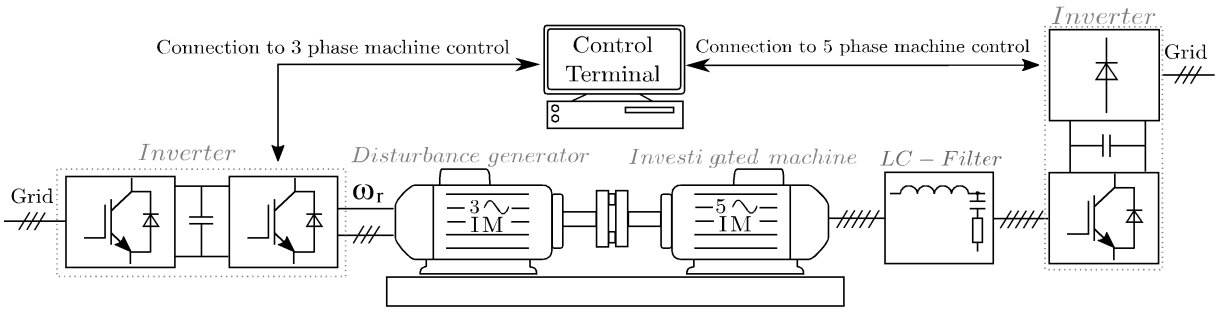

Figure 5.1: Schematic representation of the test bench with five-phase induction motor and LC filter

The disturbance generator control system was implemented based on multiscalar variables, which allowed direct control of the torque in the drive system. To generate the disturbances, the quantity $x_{12_{disturbance}}$ with varying amplitude and frequency is added to the output of the speed controller, which is the desired torque x_{12}^*. This approach provides the possibility of changing the torque appearing on the rotor shaft.

It has to be mentioned here that the experiment was performed in normal closed-loop sensorless operation, in order to take into account potential influences of the control system itself and, consequently, to simulate realistic conditions.

The investigation presents the response of the 1st plane system speed observer variable to torque changes ranging from 5 Hz to 70 Hz. The shaft speed was chosen as ω_r =0.5 p.u. to investigate the influence of the disturbances below and beyond the rotor speed frequency. To investigate the impact of the disturbances, the spectrum analysis of the estimated rotor speed and estimated load torque.

The spectrum analysis shown in Figs. 5.2 – 5.5 has the form of 3D diagrams, in which the x-axis shows the frequency analysis of the healthy state (denoted as 0 Hz), and of the introduced disturbances of 2,5 Hz, 10 Hz, 25 Hz, 50 Hz and 70 Hz. The y-axis and the z-axis represent, respectively, the variable harmonic share and the amplitude of the harmonic. In case of scale change, the visualisation is divided into two parts to facilitate identification of changes in the frequency spectrum.

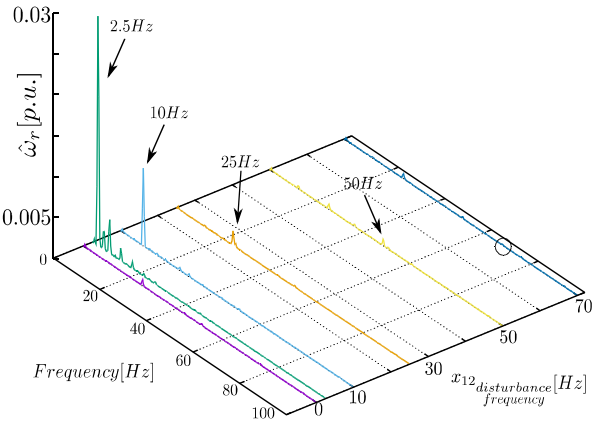

Figure 5.2: Spectral analysis of the estimated rotor speed – healthy state, 2.5 Hz and 10 Hz disturbance

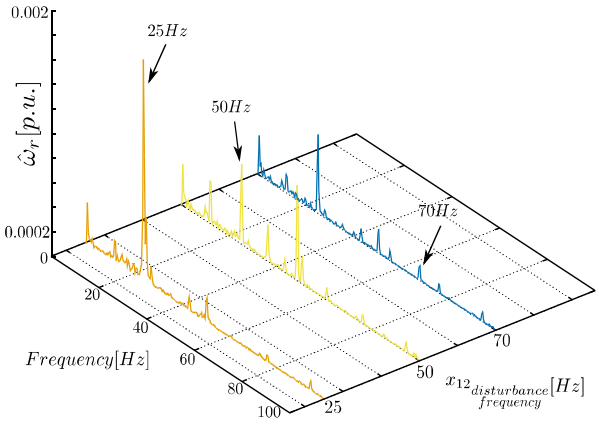

Figure 5.3: Spectral analysis of the estimated rotor speed – 25 Hz, 50 Hz and 70 Hz disturbance

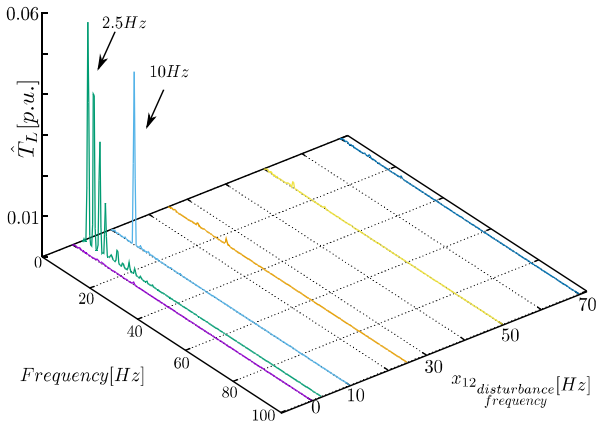

Figure 5.4: Spectral analysis of the estimated load torque – healthy state, 2.5 Hz and 10 Hz disturbance

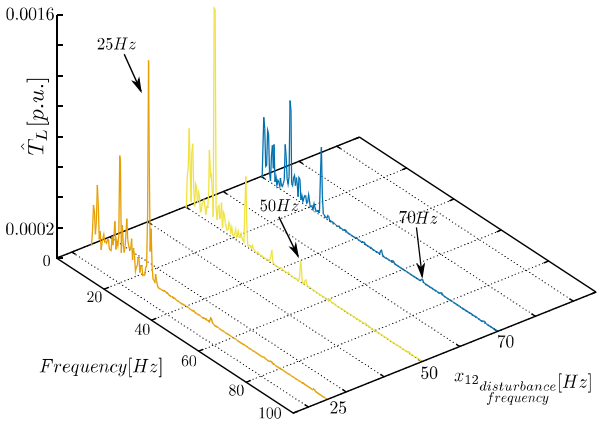

Figure 5.5: Spectral analysis of the estimated load torque - 25 Hz, 50 Hz and 70 Hz disturbance

The subharmonics that are especially noticeable in the 2.5 Hz test are caused by the rectangular disturbance signal of the load machine. This signal was used to limit the influence of the generator control system. A lower drive impact can already be seen in the scale change of the frequency analysis.

The estimated rotor speed (Figs. 5.2, 5.3) presents a strongly filtered spectrum compared to the current analysis. In the lower scale the stator frequency is dominant, along with the introduced frequencies. The 70 Hz disturbance generates a relatively low amplitude.

In the estimated load torque (Figs. 5.4, 5.5), the rotor and stator frequencies can be seen in the lower scale. Higher disturbances, beyond 50 Hz, are recognisable, but 70 Hz is hardly identifiable.

The 70 Hz harmonic is unnoticeable. Moreover, in each test a frequency of around 63 Hz occurs, which can obscure the interpretation of the drive conditions.

Summarising this experiment, it can be concluded that the presented drive disturbances are mostly visible in the estimated variables, especially in the lower frequency range of (2.5 Hz and 10 Hz). The higher frequencies (e.g. 70 Hz) are hardly visible in the spectrum. This could be related mainly to the drive setup structure, in which the inertia dampens the introduces frequencies. However, the higher amplitude disturbances are usable for a potential fault/disturbance detection algorithm.

5.2 Observer Investigations with Minor Drive Disturbances

The disturbance procedure presented in Section 5.1 was successfully implemented for higher amplitude disturbances. However, the generation of disturbances with control system implementation reveals disadvantages at very small amplitudes of torque disturbances. The reason is that the control systems of the load drive and the investigated drive compensated the disturbances in the experiment, which was an undesired effect.

To counteract the mentioned issues, the small amplitude disturbance generation is based on V/f control. However, this procedure should be performed manually with steady attention of the operator. Unlike in the V/f =const. method, this procedure allows independent control of both variables. The disturbance is generated through addition of a new harmonic with variable amplitude and frequency.

This harmonic is added to the reference value of the stator voltage magnitude and passed to the PWM procedure. The load of the machine can be regulated through the reference value of the stator voltage frequency which acts on the machine shaft. The amplitude (magnitude) of the introduced disturbance has been determined as equal to $|U|_{disturbance}$ = 0.05 p.u., in order to detect the limit of detectable faults in the torque transmission system, which is of high importance for detecting real faults at their early stages.

Fig. 5.6 presents a schematic representation of the applied disturbance procedure.

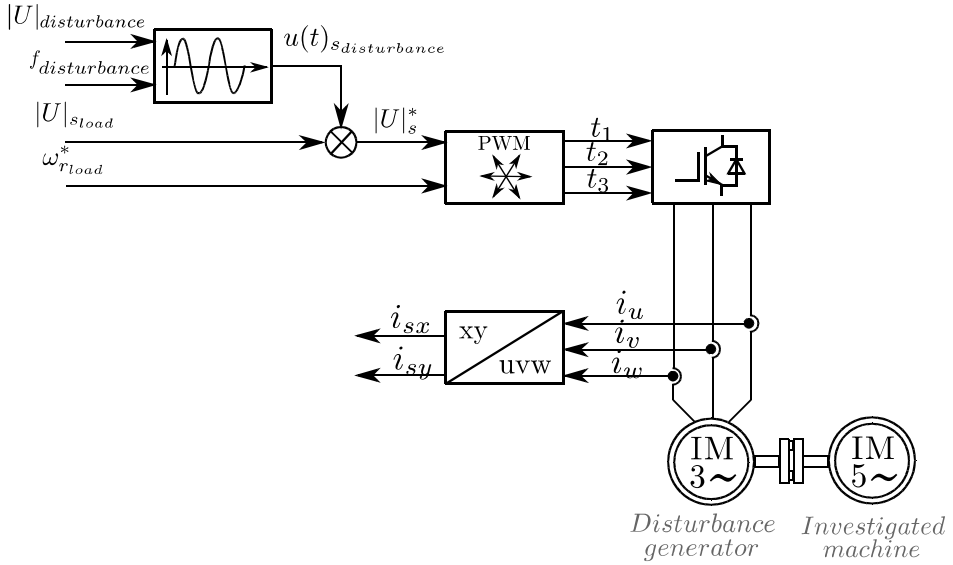

Figure 5.6: Disturbance generation with V/f control in the three-phase induction load generator

The illustrations in Figs. 5.7 – Fig. 5.8 present the frequency analysis of the observer state variables in different disturbance conditions.

The following disturbance frequencies were introduced to the drive system: healthy state (0 Hz), 2.5 Hz, 5 Hz, 10 Hz, 20 Hz and 30 Hz. These frequencies are given on the x-axis, while the z-axis and the y-axis present, respectively, the harmonic amplitude of the frequency analysis and the harmonic content. The circles ◯ in the diagram serve as support to recognise the absence or hardly visible frequencies in the spectral analysis.

The disturbance levels are relatively low in this experiment. However, the amplitude changes are well observable compared to other harmonics in the frequency spectrum.

Like in other experiments, the estimated rotor speed provides a filtered signal spectrum. The lower introduced frequencies, up to 10 Hz, are present, while the 20 Hz and 30 Hz disturbances are not recognisable.

The estimated load torque demonstrates a good insight into the disturbances up to 10 Hz, while the 20 Hz component displays a very low change and the stator frequency is recognisable.

To sum up this experiment, the introduced disturbances were at a relatively low level and did not interfere in any manner with the drive operation. However, only low frequency disturbances (<=20 Hz) could be applied for a potential disturbance/ fault detection algorithm, which may find application in drive systems with torque transmission.

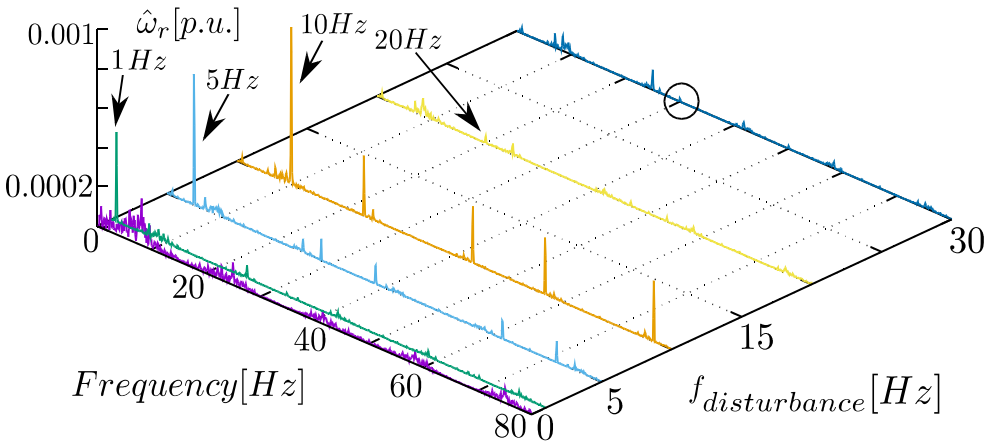

Figure 5.7: Spectral analysis of the estimated rotor speed – minor disturbances

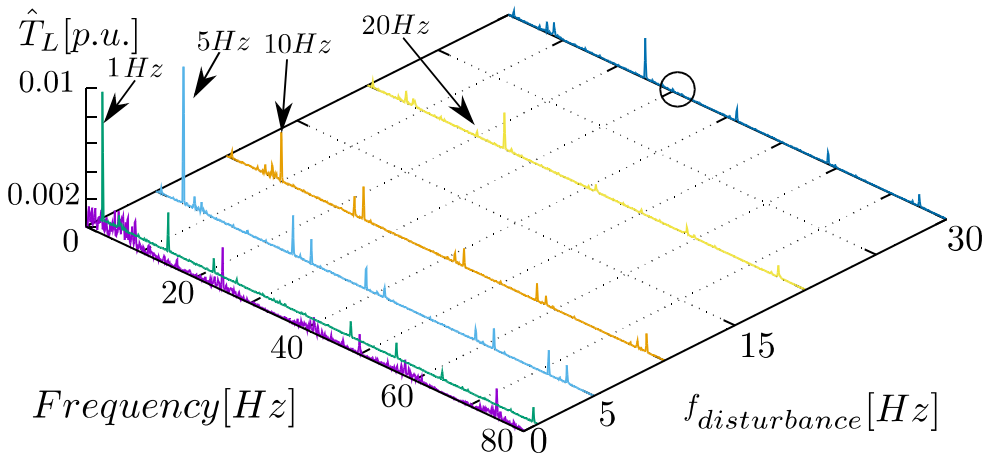

Figure 5.8: Spectral analysis of the estimated load torque – minor disturbances

5.3 Possibilities of Artificial Shaft Unbalance Fault Detection

This section demonstrates speed observer's possibilities to detect an unbalance artificially introduced to the rotor shaft. For this, an initial test setup has been prepared by the author, as presented in [18], [33]. The setup consists of a three-phase induction motor implemented with the multiscalar sensorless control system, a DC-load machine, and the vibration measurement system intended to verify the idea of detecting mechanical faults with the help of observers. The unbalance is introduced using an additional weight mounted on the rotor shaft extension, as presented in Fig. 5.9.

The first experiment focused on load torque observer estimation. After evaluation, the observer's response to the action of less intrusive unbalances in the five-phase induction motor were evaluated, including a detailed spectrum analysis of the observer variables.

The test setup consists of a three-phase induction motor with a nominal power of 1.5 kW, and additional weights that introduce unbalances to the drive. Moreover, the drive is equipped with and additional accelerometer, mounted on the stator, which monitors the physical drive behaviour of the drive.

Figure 5.9 demonstrates the unbalance introduced to the three-phase induction motor, and the accelerometer sensor used to support the drive condition measurement.

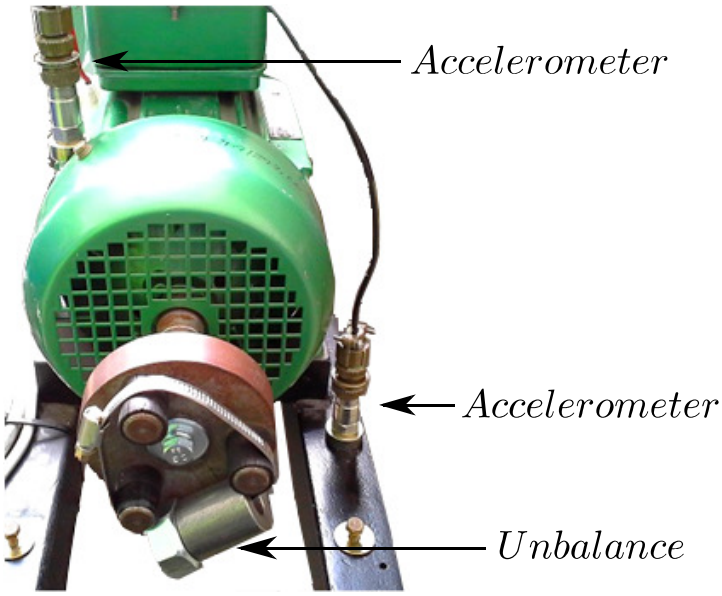

Figure 5.9: Experiment of unbalance of the three-phase induction motor with vibration measurement

The diagram in Fig. 5.10 present the vibration spectrum analysis of the drive. For this, the frequency analysis of the acceleration sensor is presented in relation to different rotor speeds. For comparison, the frequency analysis of the estimated load torque is also presented in Fig. 5.11.

After the introduction of the unbalance, the frequency spectra of vibrations and estimated load torque change significantly.

The rotor frequency related vibration amplitudes increase about 50 times or more. What is interesting here is that the peak value of the vibrations is at 22.5 Hz, and not at the nominal frequency, as might be expected from the healthy experiment.

This effect is also visible in the frequency spectrum of the estimated torque. As Fig. 5.11 indicates, the introduction of the unbalance causes a rise in the rotor frequency spectrum, which can be an indication of drive malfunction. The previous experiments positively verified the idea of fault detection with the help of the estimated load torque, by observing the measured drive vibrations.

The next experiment investigated the rotor unbalance influence on the five-phase induction motor drive with LC filter. For this, the unbalance was meaningfully reduced, and installed as presented in Fig. 5.12. This unbalance was much smaller in relation to the total moment inertia of the drive, compared to the previous experiment with the three-phase machine. The small unbalance was chosen to investigate whether such a weak symptom is extractable from the spectral analysis. In real machines, this small unbalance may result from inaccurate unbalanced masses, or early fault stages in the set of rotating blades in a ventilation system, to mention only a few.

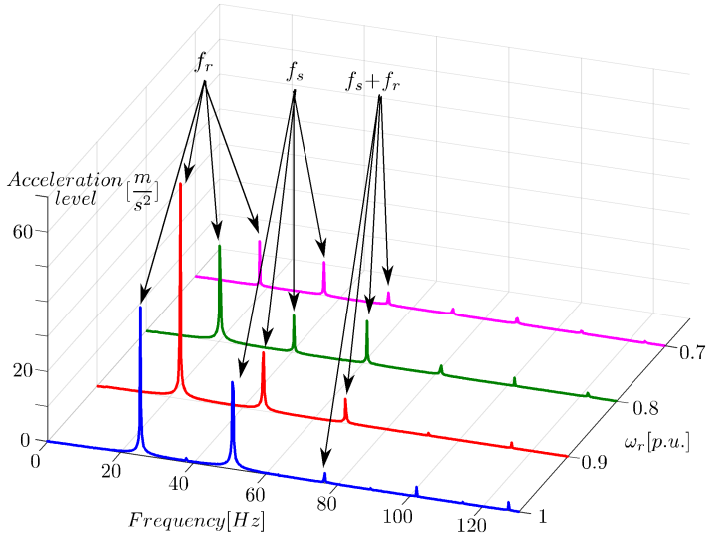

Figure 5.10: Spectral analysis of measured vibrations of the three-phase induction motor with unbalance at different rotor speeds in unloaded conditions

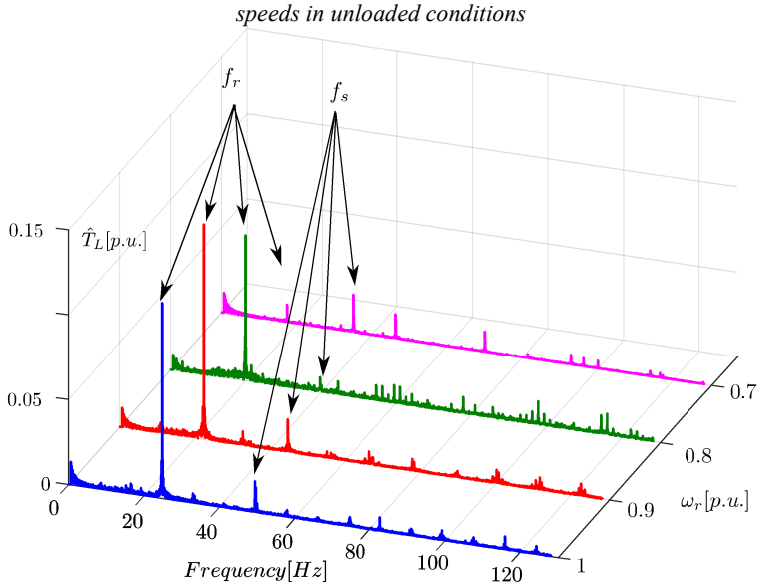

Figure 5.11: Spectral analysis of load torque of the three -phase drive with unbalance at different rotor speeds

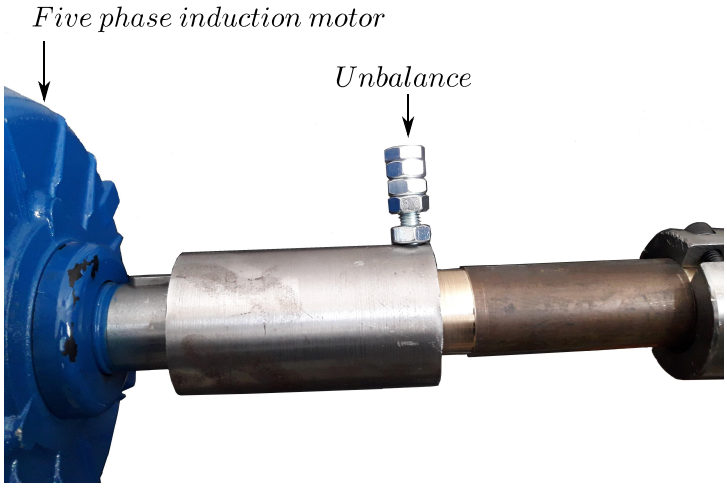

Figure 5.12: Unbalance mounted on the rotor shaft of the five-phase induction motor test setup

A use of a long screw with several mounting nuts enabled creating a reversible unbalance fault by replacing the mounting bolt with the prepared screw. The operating speed was assumed equal to ω_r=0.5 p.u. to reduce the force on the weight and without load to limit the attenuation to the observer variables. The spectral analyses in Figs. 5.13 – 5.16 demonstrate the responses of the estimated speed and load torque to the above unbalance. The differences occurring in the spectrum are marked at the harmonic with an arrow that indicates the increase (↑)or decrease (↓), compared to the healthy condition of the drive.It can be seen in the estimated rotor angular speed diagram that the rotor and stator frequency amplitudes have increased.

The estimated load torque shows a higher harmonic content in the rotor frequency range, while the double stator frequency is lower. However, the side harmonics are increased. In contrast to the 1st plane observer variables, nothing can be taken out of the frequency analysis of the 2nd plane observer variables. A lower harmonic content, without major changes, can only be recognised in the frequency spectrum. Finally, the measured rotor speed analysis shows, in contrast to expectations, a decrease of the rotor frequency amplitude and all other dominant harmonics in the spectrum.

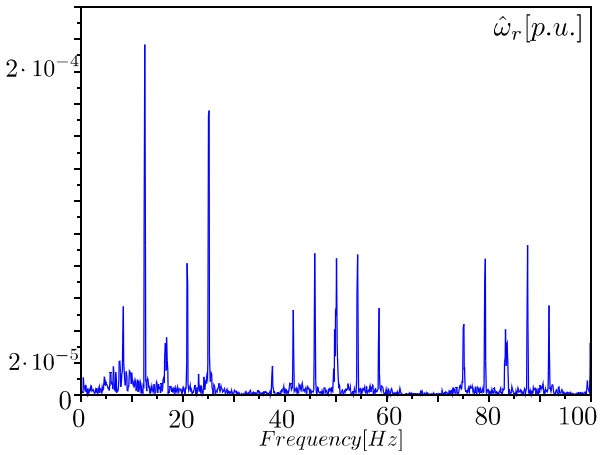

Figure 5.13: Spectral analysis of the estimated rotor speed – healthy conditions

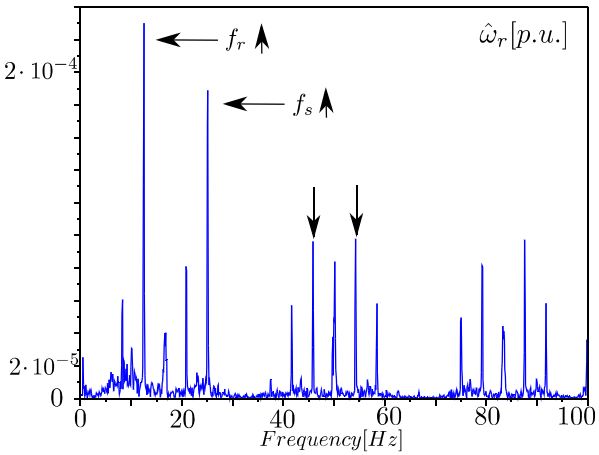

Figure 5.14: Spectral analysis of the estimated rotor speed– fault conditions

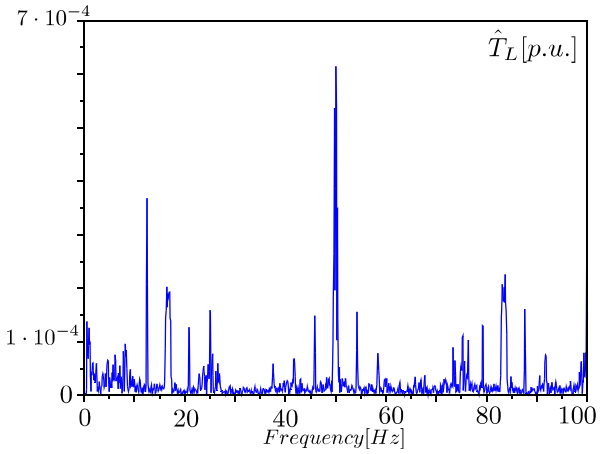

Figure 5.15: Spectral analysis of the estimated load torque – healthy conditions

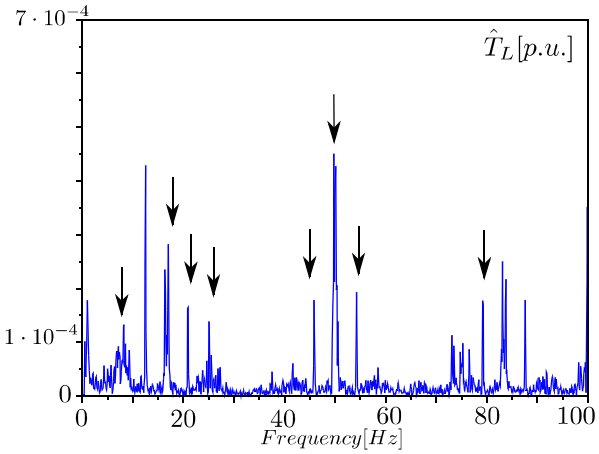

Figure 5.16: Spectral analysis of the estimated load torque– fault conditions

To sum up the experiment, the observer variables and the measured variables reveal differences in frequencies. Differences can be observed in the rotor flux variable. The increase of the rotor frequency harmonic, as well as the stator frequency and the double stator frequency amplitudes could be possibly taken into account. However, the differences in the spectrum do not present significant changes that could be used in an algorithm detecting abnormalities in the drive system. To be well identified, the unbalance fault has to provide a more significant damage to the drive system, as presented in the three-phase experiment.

5.4 Open Phase Faults

This section presents the performance investigation of the drive system with multiscalar variable based control in case of open phase faults. For this, the test setup was complemented with additional circuit breakers, mounted at filter output to simulate the phase lag in the long cable connection between filter and motor. A schematic representation of the test setup is shown in Fig. 5.17.

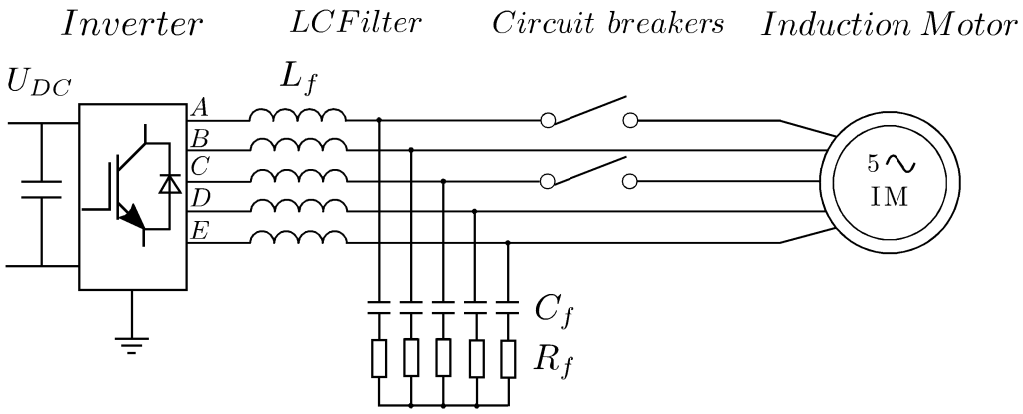

Figure 5.17: Schematic representation of open phase fault simulation for the five-phase induction motor with LC filter

The structure presented in Fig. 5.17 enables secure and fast turning off the phases. The next experiments were performed using the five-phase machine drive with closed-loop control system and with the 1st harmonic only to provide an initial insight into the drive and control system response to phase faults at light load.

Fig. 5.18 demonstrates the deactivation and reactivation of the motor stator phases. As can be seen, the deactivation of phase A does not cause any harmful interferences to the drive. However, undesired vibrations can be observed in the drive, which become even more intensive after the second phase deactivation. It can be presumed that the load torque estimation is incorrect in introducing the open phase. Nevertheless, the drive is capable of running under load without any further changes to the control system. Even the phase reactivation causes no harmful effects to the drive system.

The estimated results have shown that the system responses to phase deactivation by generating vibrations. However, the measured speed indicates that these vibrations decrease with time, and the control system returns to normal operation after the estimation stabilises.

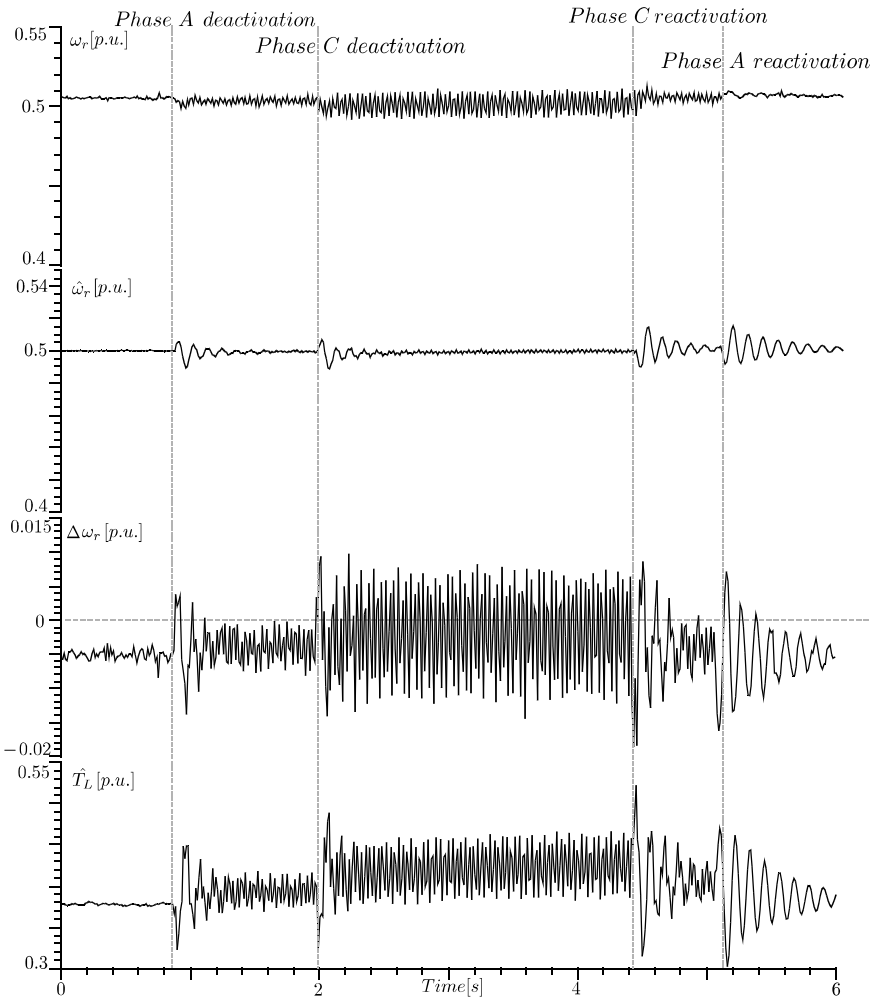

Figure 5.18: Experimental test of successive reactivation of phase A and C for 1st harmonic only under light load – measured rotor speed, estimated rotor speed, rotor speed estimation error, and estimated load torque

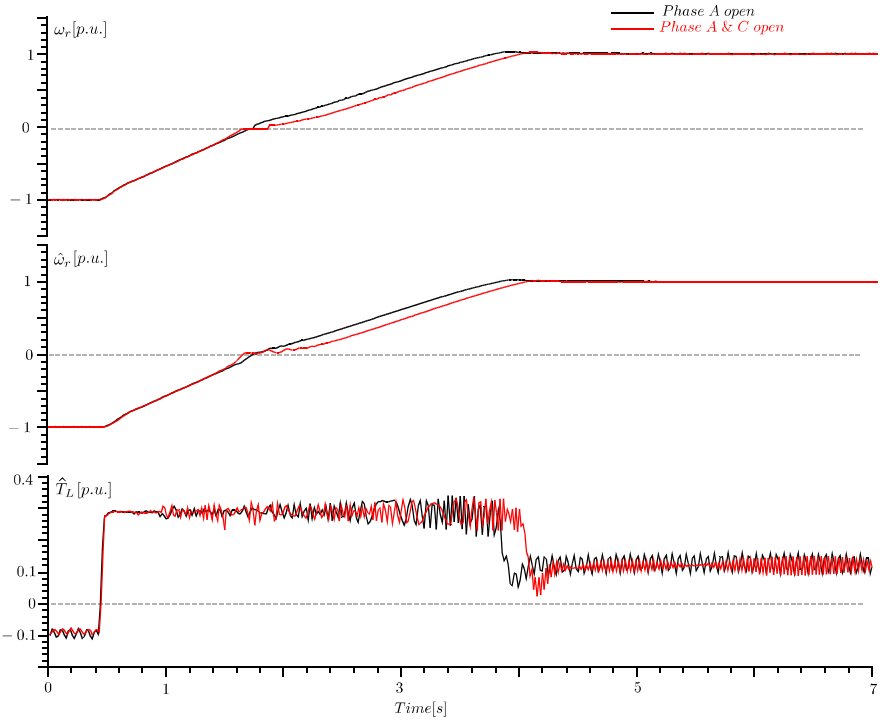

Figure 5.19: Measured rotor speed, estimated rotor speed, and estimated load torque during motor speed reverse – phase A open (black), phases A & C open (red)

Fig. 5.19 presents the motor speed reverse with phase A opened (black) and phases A and C opened (red), without load and with torque limitation of 0.3 p.u. to limit the rotor (de-)acceleration and possible over-currents during this sequence.

Remarkable here is that the unchanged control system maintains sensorless performance of the drive with inverter output filter even in the zero transition state. It can be seen that the breaking process with one or two opened phases causes no further issues. Only the value of the estimated load torque starts to oscillate at ca. $\omega_r = -0.5$ p.u. The critical zero frequency transition and the direction change are still possible, but they require more time if two phases are opened. Differences are noticeable in the start-up process, when torque is required. The start-up process took about 300 ms longer than for phase A only opened, which can also be seen on the estimated load torque.

The experiment has demonstrated that the uncritical drive operation and ability of providing torque is maintained even if one or two nonadjacent phases are opened and the control system is unchanged for this malfunctioned drive operation. This possibility is a significant difference between three-phase and five-phase drive systems, and underlines the importance of five-phase drive systems in applications which require high reliability.

5.5 Analysis of Observer Variables During Open Phase Fault

The open phase fault experiment presented in Sec. 5.4 has proved that the sensorless five-phase drive operation is possible. To illustrate the response of the observer state variables during this type of operation, the illustrations in Figs. 5.20 and 5.21 present the spectrum analysis of the observer state with open phases. In the diagrams, the x-axis indicates the healthy state, the absence of phase A, and the simultaneous absence of phase A and C.The frequency analysis of the observer variables and the measured variables gives an insight into the response of the observer variables to phase A and phase C deactivation. In the presented observer variables, after opening phase A, a harmonic appears, which is approximately twice the stator frequency. Analogously to three-phase induction motors, it can be presumed that this is related to the asymmetrical voltage supply caused by open phase faults, which changes the circular stator flux distribution and is the source of parasitic torque oscillations.

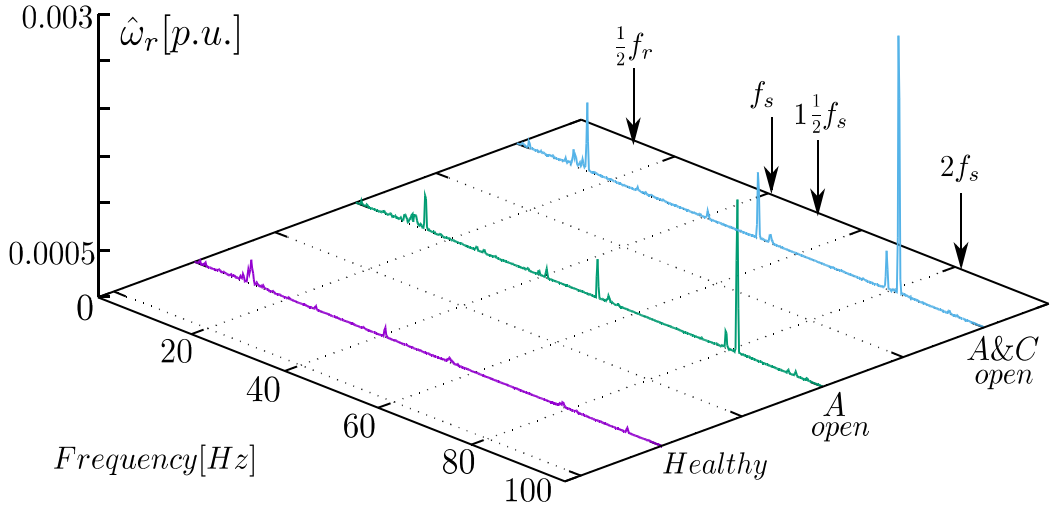

Figure 5.20: Spectral analysis of the estimated rotor angular speed – healthy state, phase A open, phases A and C open

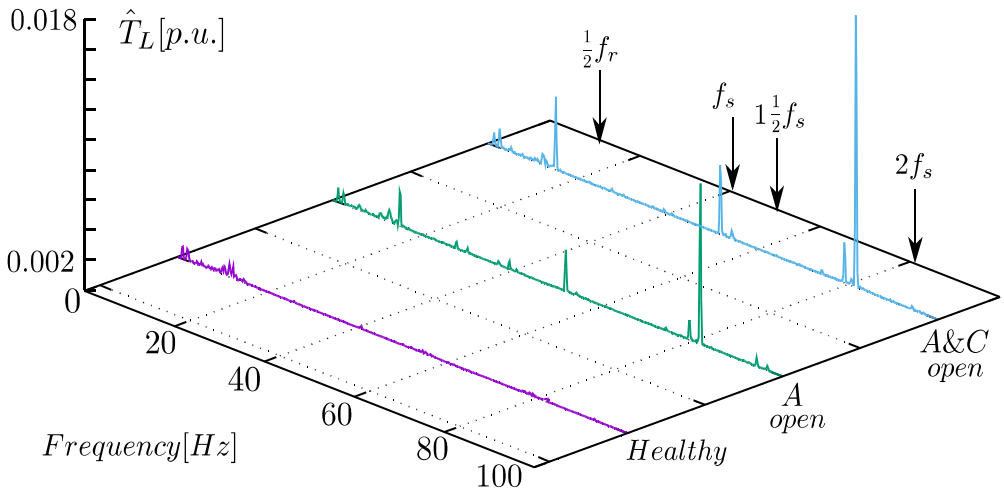

Figure 5.21: Spectral analysis of the estimated load torque – healthy state, phase A open, phases A and C open

Other harmonics appear in the ranges of 50 Hz and 15 Hz. The amplitudes of these harmonics increase after opening the second phase.

Summarising this experiment it can be concluded that uncritical post-fault operation with nonadjacent open phases is possible without further countermeasures in the control system. The drive operation remains stable even if two phases are open. Noteworthy is the stable operation of the speed observer through the zero frequency transition state (Fig. 5.19).

However, to implement a reliable post-fault tolerant control for a five-phase induction motor, several problems related to the post-fault state have to be solved. This includes the consideration of the lost switching states that decrease the number of vectors available for voltage modulation from $2^5 = 32$ to $2^4 = 16$ or even to $2^3 = 8$. Moreover, the transformation matrix from natural form to the orthogonal plane has to be changed in relation to the open phases. These countermeasures might improve the estimation of the variables during the post-fault operation, and thereby the control properties.

6 Conclusions and Future Work

The thesis presents the development of a new sensorless five-phase induction motor drive with inverter output filter and fault detection possibility by analysing observer variables. The novel control system makes use of 3rd harmonic injection to convert the air gap flux distribution into a quasi-trapezoidal shape and thus to achieve a better utilisation of the machine's magnetic circuit.

The implementation of such a drive system required introducing the 2nd control plane to provide separate drive consideration, including independent voltage generation, estimation procedure, and control system. In order to obtain the desired quasi-trapezoidal flux distribution, the 2nd control plane (virtual machine) has to operate with a three times higher frequency compared to that of the 1st control plane (main machine). However, both rotor rotor flux components have to be synchronised together.

To fulfil the requirement of sensorless control in which only the sensors implemented by default in a commercial voltage source inverter are used, a speed observer (1st plane) and a rotor flux observer (2nd plane) had to be selected and implemented.

The drive system developed in the work includes an inverter output filter, which acts beneficially for the motor lifetime and increases the application range of the drive. However, the additional LC filter increases the structural complexity of the drive, as additional elements have to be considered in the estimation process and in the control structure.

During practical realisation, the author was involved in developing the improved space vector modulation method which saved considerable calculation time. This requirement was mandatory to overcome technical limitations of the DSP.

The DSP and FPGA systems used in the experiment offered limited possibilities and required certain code optimizations with respect to their execution times to reach the objectives of the dissertation.

The calculations that were required to be executed within 150 μs included SVM, 21 differential equations, transformation matrices, ADC scaling, and the control system with nine PI controllers.

The implemented observers operated in the full speed range and showed no negative issues at low speed, during direction changes, and during zero speed/frequency transitions. Furthermore, the applied speed observer estimated the rotor angular speed with relatively low error (excluding the low speed operation), equal to or below 4%, during transitions and about 0.2% in the steady state. This was a remarkable achievement considering the presence of the inverter output filter, which contributed to significantly higher complexity of the sensorless control structure.

The consideration of the inverter output filter inductance in the control structure was implemented using the solution proposed by the author. This solution is based on filtrating the filter inductance current that is already calculated in the observer structure. The filter inductance voltage drop calculation was added to the reference voltage module, which as a result supported the control system and compensated the voltage drop. This method was indispensable, as it used only a fraction of the computing time compared to other methods that require more transformation matrices and/or more PI controllers which have to be tuned.

The fault detection investigations were based on the spectral analysis of the estimated variables, which provided an insight into their harmonic contents. It could be seen that the introduced harmonics were identified in the frequency analysis, especially in the lower frequency range.

The frequency analysis of the estimated and measured values which was performed in this experiment allowed to detect the introduced frequencies, which were dominant in the low frequency range and less noticeable for higher frequency disturbances. This experiment led to further fault detection investigations, which included, in particular, artificial unbalance of the drive shaft.

The final experiments were dedicated to the problem of open phase faults in a five-phase induction motor system with LC filter, and revealed an enormous reliability potential of the five-phase drive.

The possibility of providing torque, even with one or two phases opened, was presented and complemented with the response analysis of the estimated variables in different motor operations. The analysis of the estimated variables has demonstrated that a dominant harmonic with twice the stator frequency arises and this harmonic definitively indicates the fault state of the machine.

Regarding the presented open-phase tests, it can be concluded that the possibility of operating a five-phase machine with the absence of one or even two nonadjacent phases will presumably require consideration of the post-fault state in terms of available voltage vectors and changes in the transformation matrix to the orthogonal planes. These countermeasures might improve the control and variable estimation during the post-fault operation.

High potential of this topic has motivated the author to plan future work which will focus on studying different observer and estimator structures to improve control properties.

This will require the use of a more powerful processor unit which will make use of multiple cores and moving possible calculations from the processor to the FPGA with shared memory for calculation results. Regarding the control system, the author plans in future to work on optimisation of the synchronisation procedure and more enhanced consideration of the LC filter. Concerning the fault detection possibilities, the author is motivated to redesign the load torque observer and complement it with a detailed model of the mechanical system for dedicated abnormality detection in the drive system. Moreover, the open phase possibilities of the five-phase induction motors motivated the author as well to work on further modifications of control structures for post-fault operation.

It can be assumed that the new knowledge gained in the studies reported in the dissertation will help in further variable estimation based drive implementations, especially in sensorless five-phase drives with high reliability and fault detection possibility.

In line with the PhD dissertation, the author supervised the research project of the National Science Centre of Poland, entitled "Sensorless identification of mechanical faults of a multiphase drive system with inverter output filter" and completed in 2018. The test setup was designed and built by the author during the realisation of projects objectives. A large percentage of the experimental outcome of this research is investigated in this dissertation.

Furthermore, the drive system with five-phase induction motor and voltage source inverter was presented by the author at the international exhibition “Hannover Messe” in Germany in 2017, at the fair stand of the representation of Poland, as well as on the Polish exhibition EXOPOWER in Poznań in 2017. In 2018, the drive system was presented in Kraków (Impact'18) and in Katowice (Impact mobility rEVolution'18). In each case the drive system aroused high interest, which underlines the importance and the current relevance of the investigated topic.

References

[1] F. Blaschke, “A new method for the structural decoupling of A.C. induction machines,” in *Conf. Rec. IFAC*, Düsseldorf Germany, 1971.

[2] M. P. Kaźmierkowski, R. Krishnan, and F. Blaabjerg, *Control in power electronics: selected problems*. Academic press, 2002.

[3] M. Depenbrock, “Direct self-control (DSC) of inverter-fed induction machine,” *IEEE Trans. Power Electron.*, vol. 3, no. 4, pp. 420–429, Oct. 1988.

[4] Z. Krzeminski, “Nonlinear Control of Induction Motor,” in *10th IFAC Congress on Automatic Control*, 1987, pp. 349–354.

[5] Z. Liu, Y. Li, and Z. Zheng, “A Review of Drive Techniques for Multiphase Machines,” *China Electrotech. Soc. Trans. Electr. Mach. Syst.*, vol. 2, no. 2, Jun. 2018.

[6] H. Guzman, J. A. Riveros, M. J. Duran, and F. Barrero, “Modeling of a five-phase induction motor drive with a faulty phase,” in *2012 15th International Power Electronics and Motion Control Conference (EPE/PEMC)*, Novi Sad, Serbia, 2012, p. LS1c.3-1-LS1c.3-6.

[7] J. Riveros, B. Bogado, J. Prieto, F. Barrero, S. Toral, and M. Jones, “Multiphase machines in propulsion drives of electric vehicles,” in *Power Electronics and Motion Control Conference (EPE/PEMC), 2010 14th International*, 2010, pp. T5–201.

[8] I. Bolvashenkov, J. Kammermann, S. Willerich, and H.-G. Herzog, “Comparative study of reliability and fault tolerance of multi-phase permanent magnet synchronous motors for safety-critical drive trains,” in *Proceedings of the International Conference on Renewable Energies and Power Quality (ICREPQ’16)*, 2016, vol. 4, pp. 1–6.

[9] F. Terrien, S. Siala, and P. Noy, “Multiphase induction motor sensorless control for electric ship propulsion,” in *Proc. IEE PEMD Conf., Edinburgh, UK*, 2004, pp. 556–561.

[10] E. E. Ward and H. Härer, “Preliminary investigation of an invertor-fed 5-phase induction motor,” in *Proceedings of the Institution of Electrical Engineers*, 1969, vol. 116, pp. 980–984.

[11] E. Levi, R. Bojoi, F. Profumo, H. A. Toliyat, and S. Williamson, “Multiphase induction motor drives - a technology status review,” *IET Electr. Power Appl.*, vol. 1, no. 4, p. 489, 2007.

[12] J. Guzinski, G. Kostro, P. Strankowski, M. Morawiec, and F. Wilczyński, “Drive Properties of Five-phase Squirrel Cage Induction Motor - Właściwości napędowe pięciofazowego silnika indukcyjnego klatkowego - in Polish,” *Autom. Elektr. Zakłócenia*, no. Innowacje, pomiary i bezpieczeństwo w elektroenergetyce, pp. 14–26, 2017.

[13] M. Adamowicz, J. Guzinski, and Z. Krzeminski, “Nonlinear control of five phase induction motor with synchronized third harmonic flux injection,” in *Smart Grid and Renewable Energy (SGRE), 2015 First Workshop on*, 2015, pp. 1–6.

[14] M. Adamowicz, Z. Krzeminski, M. Morawiec, P. Strankowski, and J. Guziński, “Multiscalar Control of Five-Phase Induction Motor - Sterowanie multiskalarne pieciofazową maszyną indukcyjną - in Polish,” *Przegląd Elektrotechniczny*, vol. 1, no. 5, pp. 108–115, May 2016.

[15] M. Adamowicz, P. Strankowski, J. Guzinski, and Z. Krzeminski, “Multiscalar Control of Five-Phase Induction Motor - Sterowanie multiskalarne pięciofazowym silnikiem indukcyjnym - in Polish,” in *XII Krajowa Konferencja Naukowa Sterowanie w Energoelektronice i Napędzie Elektrycznym SENE*, Łódź, 2015.

[16] J. Guzinski *et al.*, “Sensorless multiscalar control of five-phase induction machine with inverter output filter,” 2017, p. P.1-P.10.

[17] M. Morawiec, P. Strankowski, A. Lewicki, and J. Guzinski, “Sensorless control of five-phase induction machine supplied by the VSI with output filter,” in *2016 10th International Conference on Compatibility, Power Electronics and Power Engineering (CPE-POWERENG)*, 2016, vol. 48, pp. 304–309.

[18] J. Guzinski, H. Abu-Rub, and P. Strankowski, *Variable Speed AC Drives with Inverter Output Filters*. John Wiley & Sons, 2015.

[19] J. Salomäki, “Sensorless Control of AC Drives Equipped With An Inverter Output Filter,” Helsinki University of Technology, 2007.

[20] Z. Krzeminski, “Speed Observers for Sensorless Control of AC Machines - Obserwatory prędkości dla bezczujnikowego sterowania maszynami prądu przemiennego - in Polish,” *Przegląd Elekrotechniczny*, vol. 5, p. 14, 2014.

[21] J. Guziński, *Induction Motor Drive Systems with Inverter Output Filters: Selected Problems -Układy napędowe z silnikami indukcyjnymi i filtrami wyjściowymi falowników: zagadnienia wybrane - in Polish*. Gdańsk: Wydawnictwo Politechniki Gdańskiej, 2011.
[22] H. Lutz and W. Wendt, *Handbook of Control Systems: with MATLAB and Simulink -Taschenbuch der Regelungstechnik: mit MATLAB und Simulink - German*, 7., Aufl. Frankfurt am Main, 2007.
[23] T. Senjyu, E. B. Muhando, A. Yona, N. Urasaki, H. Kinjo, and T. Funabashi, "Maximum Wind Power Capture by Sensorless Rotor Position and Wind Velocity Estimation from Flux Linkage and Sliding Observer," *Int. J. Emerg. Electr. Power Syst.*, vol. 8, no. 2, Jan. 2007.
[24] T. Senjyu, T. Shingaki, and K. Uezato, "Sensorless vector control of synchronous reluctance motors with disturbance torque observer," *IEEE Trans. Ind. Electron.*, vol. 48, no. 2, pp. 402–407, Apr. 2001.
[25] T. Ohtani, N. Takada, and K. Tanaka, "Vector control of induction motor without shaft encoder," *IEEE Trans. Ind. Appl.*, vol. 28, no. 1, pp. 157–164, 1992.
[26] J. Hu and B. Wu, "New integration algorithms for estimating motor flux over a wide speed range," in *PESC97. Record 28th Annual IEEE Power Electronics Specialists Conference. Formerly Power Conditioning Specialists Conference 1970-71. Power Processing and Electronic Specialists Conference 1972*, St. Louis, MO, USA, 1997, vol. 2, pp. 1075–1081.
[27] Kun Zhao and Xiaojie You, "Speed estimation of induction motor using modified voltage model flux estimation," in *2009 IEEE 6th International Power Electronics and Motion Control Conference*, Wuhan, 2009, pp. 1979–1982.
[28] Z. Krzeminski, "Observer of induction motor speed based on exact disturbance model," in *Power Electronics and Motion Control Conference, 2008. EPE-PEMC 2008. 13th*, 2008, pp. 2294–2299.
[29] J. Guziński, H. Abu-Rub, and P. Strankowski, "Speed Sensorless AC Drive with Inverter LC Filter and Fault Detection Using Load Torque Signal," *Przegląd Elekrotechniczny*, vol. 1, no. 2, pp. 291–299, Feb. 2017.
[30] Z. Krzeminski, *Digital Control of Asynchronous Machines - Cyfrowe sterowanie maszynami asynchronicznymi - in Polish*, Monograph. Gdansk University of Technology, 2000.
[31] F. Wilczynski, P. Strankowski, J. Guzinski, M. Morawiec, and A. Lewicki, "Vector control of five phase induction rotor with rotor flux shape optimization - Sterowanie wektorowe pięciofazowym silnikiem indukcyjnym z optymalizacją rozkładu strumienia wirnika - in Polish," *Wiad. Elektrotechniczne*, no. 11/2017, pp. 23–28.
[32] Huangsheng Xu, H. A. Toliyat, and L. J. Petersen, "Five-phase induction motor drives with DSP-based control system," *IEEE Trans. Power Electron.*, vol. 17, no. 4, pp. 524–533, Jul. 2002.
[33] P. Strankowski and J. Guziński, "Sensorless Mechanical Fault Diagnosis in Electrical Drives with Inverters - Bezczujnikowa diagnostyka uszkodzeń mechanicznych w przekształtnikowym napędzie elektrycznym - in Polish," *Napędy Sterow.*, vol. 17, no. 5, pp. 84–88, 2015.